AFRL-IF-RS-TR-1998-185
Final Technical Report
September 1998
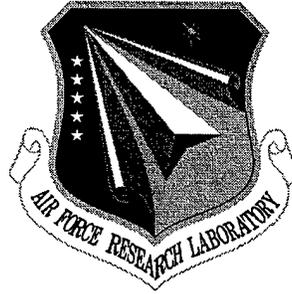
ADVANCED TECHNOLOGY IMPLEMENTATION FOR SURVEILLANCE RADARS

Research Associates for Defense Conversion, Inc.

Tzeta Tsao, Braham Himed, and Adel Slamani

APPROVED FOR PUBLIC RELEASE; DISTRIBUTION UNLIMITED.

19981104 035

**AIR FORCE RESEARCH LABORATORY
INFORMATION DIRECTORATE
ROME RESEARCH SITE
ROME, NEW YORK**

DTIC QUALITY INSPECTED 4

This report has been reviewed by the Air Force Research Laboratory, Information Directorate, Public Affairs Office (IFOIPA) and is releasable to the National Technical Information Service (NTIS). At NTIS it will be releasable to the general public, including foreign nations.

AFRL-IF-RS-TR-1998-185 has been reviewed and is approved for publication.

APPROVED:

DAVID D. FERRIS, JR.
Project Engineer
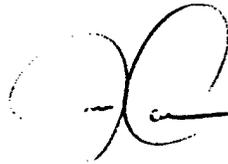
FOR THE DIRECTOR:

JOSEPH CAMERA, Deputy Chief
Information & Intelligence Exploitation Division
Information Directorate

REPORT DOCUMENTATION PAGE			*Form Approved* OMB No. 0704-0188

Public reporting burden for this collection of information is estimated to average 1 hour per response, including the time for reviewing instructions, searching existing data sources, gathering and maintaining the data needed, and completing and reviewing the collection of information. Send comments regarding this burden estimate or any other aspect of this collection of information, including suggestions for reducing this burden, to Washington Headquarters Services, Directorate for Information Operations and Reports, 1215 Jefferson Davis Highway, Suite 1204, Arlington, VA 22202-4302, and to the Office of Management and Budget, Paperwork Reduction Project (0704-0188), Washington, DC 20503.

1. AGENCY USE ONLY *(Leave blank)*	2. REPORT DATE September 1998	3. REPORT TYPE AND DATES COVERED Final May 95 - Feb 98	

4. TITLE AND SUBTITLE	5. FUNDING NUMBERS
ADVANCED TECHNOLOGY IMPLEMENTATION FOR SURVEILLANCE RADARS	C - F30602-95-C-0121 PE - 61102F
6. AUTHOR(S) Tzeta Tsao, Braham Himed, and Adel Slamini	PR - 2304 TA - E8 WU - PE

7. PERFORMING ORGANIZATION NAME(S) AND ADDRESS(ES) Research Associates for Defense Conversion, Inc. 10002 Hillside Terrace Marcy NY 13441-4514	8. PERFORMING ORGANIZATION REPORT NUMBER N/A

9. SPONSORING/MONITORING AGENCY NAME(S) AND ADDRESS(ES) AFRL/IFEA 32 Brooks Road Rome NY 13441-4114	10. SPONSORING/MONITORING AGENCY REPORT NUMBER AFRL-IF-RS-TR-1998-185

11. SUPPLEMENTARY NOTES

AFRL Project Engineer: David Ferris/IFEA/(315) 330-4408

12a. DISTRIBUTION AVAILABILITY STATEMENT Approved for public release; distribution unlimited	12b. DISTRIBUTION CODE

13. ABSTRACT *(Maximum 200 words)*

This report presents an analysis of the clutter characteristics as observed from a radar platform either the monostatic or the bistatic configuration, airborne or stationary. The study shows the effects of the system parameters, particularly the system geometry, on the observed clutter characteristics.

A preliminary study of adaptive space-time processing for multistatic active radar is also included in the report. There are two major factors that need to be investigated further development of space-time processing for the multistatic system; (1) the correlation of the observed interference among the receivers; and (2) the effects of system geometry on the observed reverberation characteristics. The analysis shows that problem interferences are uncorrelated. However, this may not be the case when multipath occurs.

14. SUBJECT TERMS Space-time Adaptive Processing, Non-Gassian Clutter, Bistatic/Multistatic Radar			15. NUMBER OF PAGES
			16. PRICE CODE

17. SECURITY CLASSIFICATION OF REPORT UNCLASSIFIED	18. SECURITY CLASSIFICATION OF THIS PAGE UNCLASSIFIED	19. SECURITY CLASSIFICATION OF ABSTRACT UNCLASSIFIED	20. LIMITATION OF ABSTRACT UL

Executive Summary

Characteristics of ground clutter in stationary and airborne radar systems is studied herein. Both the monostatic and bistatic configuration are considered. The focus is on how the clutter characteristics are affected by the manner in which observation is performed. The factors considered include the transmitted waveform, pulse compression, radar platform motion. antenna pattern, and system geometry.

The analysis starts with a brief review of the space-time processing. This review also shows the manner in which clutter estimation is involved in the space-time processing. The basic model for the clutter analysis is then presented. It is followed by the derivation of the clutter autocorrelation function for three cases. namely, clutter observed from a stationary monostatic radar, from an airborne monostatic radar, and from an airborne bistatic radar.

It should be pointed out that, in this study. no consideration is given to the variation in clutter strength due to the different incidence and observation angles. However, this problem cannot be solved until a constant Gamma model is developed, and verified through experiment, for the out-of-plane clutter in bistatic configuration. The assumption about the scatterer spectrum may also be relaxed to allow for the derivation of clutter process from basic principles, especially for the derivation of non-Gaussian clutter.

The goal of this effort is two-fold. First. through the analysis of the effects of the system parameters on the clutter characteristics, criteria for secondary data selection and for signal design in space-time processing can be developed. Another application of this analysis is that it provides as a basis for the development of the space-time processing for bistatic/multistatic radars. A preliminary study is presented in this report to show how the multistatic case departs from its monostatic counterpart. The procedure for further development is also discussed.

List of Figures

Chapter 1

Introduction

Detection of slowly moving objects close to the ground or sea surface by means of an airborne radar is seriously impaired by clutter returns. These returns exhibit Doppler shift which varies with the velocity of the radar platform and the direction of the antenna beam. In addition, even absolutely stationary clutter has a Doppler spectrum due to the fact that reflections of scatterers from different parts of the beam have different Doppler shifts.

Clutter cancellation is effectively achieved by filtering out the portion of the Doppler spectrum occupied by the clutter return. However, the target may also be eliminated in the process if Doppler is the only condition used to distinguish the clutter and the target, since the sidelobe clutter may overlap the target. This problem is encountered by the traditional Moving Target Indicator (MTI). In contrast, adaptive space-time processing further distinguishes the clutter and the target return in the angle dimension by employing arrays of sensors. Thus, by assigning appropriate weights to the sensors, the notch of the clutter cancellation filter is placed along the line where the clutter lies in the angle-velocity plane.

To select the weights to the sensors, it was shown that the weights which maximize the signal-to-clutter-plus-noise ratio (SCNR) are related to the clutter covariance. In practice, however, the clutter covariance is substituted with its estimate when forming the weights, since this quantity is generally not known a priori. This estimate is obtained from clutter samples in real-time. As a result, space-time processing greatly improves the output signal-to-noise ratio with minimal a priori information about the changing environment.

Numerous research efforts from both the radar and the sonar communities have been

1

devoted to the analysis of space-time processing. Development of this scheme still lacks in two areas, however. First, there are few studies for the bistatic/multistatic systems in the open literature. This type of system configuration consists of one or multiple transmitters and receivers that are separated in space. The advantage is the decreased vulnerability over its monostatic counterpart; nevertheless, the increased complexity in system geometry introduces difficulties for effective realization and analysis.

Another area of the space-time processing scheme that requires further investigation is how the performance is affected by the clutter statistical estimation. This question is of concern especially when spatial averaging is involved in the clutter estimation, since clutter from different locations may not have the same spectrum.

In this research effort we consider the aforementioned two problems, but the emphasis is on the study of the problems associated with clutter estimation. To set the stage for later development, we give in the following a brief review of how the space-time processing was derived for the monostatic system. In Section 2 we describe the assumptions and methodology used in analyzing the clutter statistical characteristics. In Chapter 2, we study the clutter characteristics as observed from a stationary monostatic system, an airborne monostatic system, and an airborne bistatic system. In Chapter 3, we examine how the Doppler spread in the ground clutter affects the clutter spectrum and clutter correlation function. A preliminary study of space-time adaptive processing for bistatic/multistatic is given in Chapter 4. Chapter 5 discusses the results.

1.1 Space-time processing in monostatic radar system

In this section we briefly review the manner in which space-time processing was derived for the monostatic radar system. The treatment follows closely to that given in [1].

Filtering of the received signal to improve the signal-to-clutter-plus-noise ratio is essential to the detection of a moving target close to the ground or sea. However, schemes which involve processing only in the time or the frequency domain are ineffective; they may remove both the clutter and the target when the sidelobe clutter exhibits the same Doppler as the

target. This situation is illustrated in Figure 1.1, where v and V are the speed of the radar platform and of the target, respectively. φ and θ are the azimuth and the depression angles, respectively, and λ is the wavelength. For simplicity, we assume the depression angle is small.

In most cases, the clutter and the target can be further distinguished in the angular dimension, as depicted in Figure 1.2. This figure shows that the added degree of freedom in clutter processing enables one to avoid the problem of rejecting both the clutter and the target. Clearly, the angular information can be obtained when an array of sensors is used.

Suppose that the echo from a target is received by a set of N sensors. Let each sensor yield K temporal samples of the received signal such that a total of $L = N \times K$ samples are obtained at the receiver. Further assume that the sampling is performed at the I/Q channel output. Denote the entire sample data set by the column vector $s = [s_1 \, s_2 \cdots s_L]^T$, where $s_k, k = 1, 2, \cdots, L$ is the kth signal sample and the superscript T denotes the transpose operation. Similarly, denote the noise vector by $n_c = [n_1 \, n_2 \cdots n_L]^T$. Further, let M_{n_c} denote the noise covariance matrix. The detection of the presence of a target is by putting the received vector through a filter with weights $w = [w_1 \, w_2 \cdots w_L]^T$.

The output signal-to-noise ratio of the filter is given by

$$d^2 = \frac{\left| w^H s \right|^2}{w^H M_{n_c} w} \tag{1.1}$$

where H denotes the Hermitian operation. Using the Schwarz inequality, it can be shown [1] that d^2 is maximized by

$$w = k M_{n_c}^{-1} s \tag{1.2}$$

where k is a constant not equal to zero. It can also be shown [1] that the weights given by (1.2) maximize the detection probability, at a given false alarm rate, in a Gaussian noise environment.

Realization of (1.2) requires the knowledge of M_{n_c}. Since M_{n_c} is seldom known a priori, it needs to be estimated. Denote the estimate of M_{n_c} by $\hat{M}_{n_c}$. Thus, the weights to the
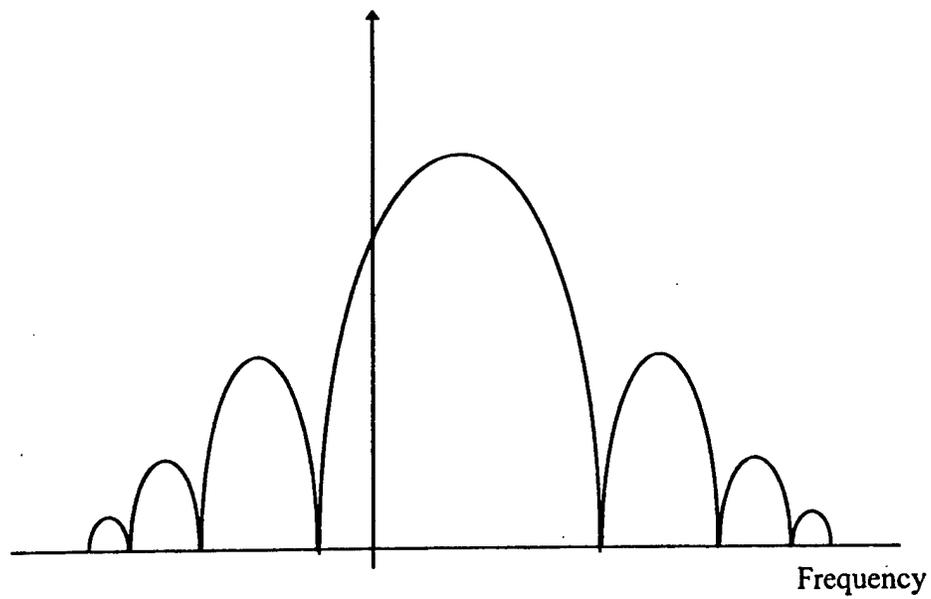
Figure 1.1: Clutter Doppler spectrum for airborne monostatic radar.
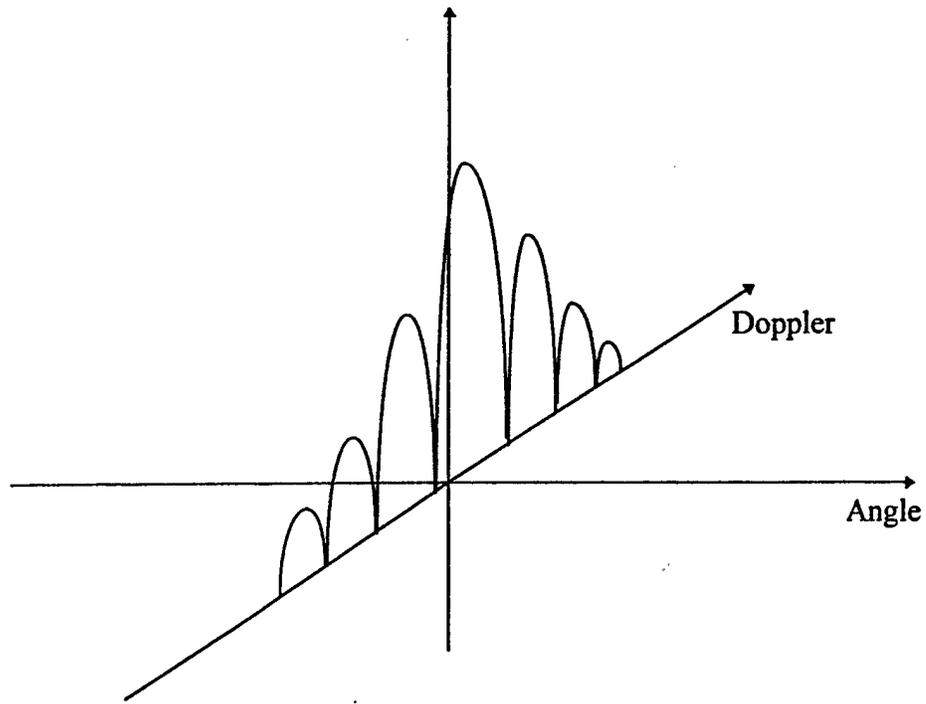
Figure 1.2: Clutter in the angle-Doppler space

sensors are actually calculated from

$$w = k\tilde{M}_{n_c}^{-1}s \tag{1.3}$$

There are two methods commonly used for the estimation of the clutter covariance matrix. One is to use the sample covariance matrix, which is the maximum likelihood estimate for the Gaussian clutter. Another approach is the maximum entropy method (MEM), which involves the estimation of the clutter power spectrum. With either method, spatial averaging across several range cells is generally to increase the available samples, under the assumption that the clutter is homogeneous in a close neighborhood. However, clutter samples obtained from different range cells correspond to clutter return from different range, while clutter returns from different range may not have the same Doppler spectrum due to the factors previously described. The geometry effects on the matched filter output due to a point target was analyzed in [2]. In the next chapter we will consider the factors that affect the clutter statistical characteristics.

Another part of the realization of (1.2) is the choice of *s*. This choice has the effect of canceling out the undesired interference and is called a steering signal. To illustrate the use of steering signals, consider the following. Assume the array is linear with sensor element spacing *l*. Then, the relative phase of the *k*th sensor due to a signal arriving at an angle φ with respect to the array normal is given by

$$\psi_k = \frac{2\pi(k-1)l}{\lambda}\sin\varphi, k = 1, 2, \cdots, N \tag{1.4}$$

The above relationship indicates that signal arriving in different directions induces different relative phases among the sensors . This feature is exploited by adjusting the phases of $\tilde{s}$ to tune out the undesired interference. In Chapter 5 we present a preliminary study of how the above analysis can be extended to the multistatic case.

1.2 Basic model for clutter analysis

In this section we discuss the assumptions and methodology commonly adopted in the literature on the analysis of clutter. This consideration provides us with a basis for the devel-

opment of a statistical description of the clutter, to be used in our study of the estimation performance and the effects on the space-time processing.

The most adopted assumption about clutter is that the clutter is a collection of independent point scatterers. The number and reflectivity of the scatterers are then modeled as random numbers. The appropriate assignment of the underlying probability distribution for different types of terrain have been the subject of many research efforts. The occurrence of a scatterer in time is generally assumed to be governed by Poisson process, e.g., in [3]. This assumption leads to Gaussian clutter by further assuming that the number of scatterers is large. Other models for the number of the scatterers were also proposed in the literature. In particular, a recent paper [4] shows that clutter of Spherically Invariant family can be obtained by using Poisson mixture distribution.

There are system factors which affect clutter characteristics. Clearly, the ground area illuminated depends on the transmitting and receiving apertures and the system geometry. The size of a resolution cell also determines how many scatterers contribute to the clutter return [5]. Furthermore, the clutter spectrum is a function of the relative motion between the scatterers and the radar platform. Finally, there is the effect of the relative position of the scatterers and the radar platform, which affects the strength of the reflections, as well as the location and shape of the clutter spectrum. A rather thorough treatment on the effects of these factors can be found in Middleton's work [6]-[10].

Our analysis will differ from the previous work in two aspects: we will include pulse compression and give an explicit description of the geometry relationships. In modern radars, pulse compression is used to improve the resolution capability. Pulse compression is achieved through raising the bandwidth of the signal by modulation, at transmission, and matched filtering, at reception. As a result, the samples available, i.e., the output of each range resolution cell, are the result of matched filtering. Thus, it is of interest to know how the estimated clutter characteristics are subjected to change due to matched filtering, as compared to using samples from sampling the received signal directly.

Another issue which is generally overlooked is an explicit derivation of the geometry relationships. Rather than giving a set of equations to describe the geometry, we will solve

7

them explicitly and discuss the implications. This will lend some insight as how system performance varies with geometry.

Specifically, we will assume that the transmitted signal is a periodic pulse sequence. Reflection from the ground is modeled as a doubly-spread return [11]. This is a modification to Klemm's approach used in [12], where the clutter from one range cell is modeled as a Doppler-spread return. One recent work adopted a similar approach [13]. The clutter return is assumed to be the superposition of reflections from a number of independent point scatterers. At any instant, the region from where the scatterers contribute to the clutter return corresponds to the extension of one range resolution cell, which is obtained from pulse compression. The spatial distribution of the scatterers is governed by a probability density function. The number, n, and the reflectivity, g, of the scatterers are modeled as random numbers. The strength of the reflections also depend on the antenna transmit pattern G_T and receive pattern G_R, the transmitted waveform $s(t)$, and the distance the signal traveled.

We further have the following assumptions. First, the terrain is assumed to be flat [14]. The range of depression angle of interest is assumed small such that the range resolution is determined by the signal pulse duration [15]. Range ambiguities are not considered at present analysis. The probability density function describing the location of the scatterers does not change within the observation interval. The fluctuation of the reflectivity of the scatterers during the observation interval can be modeled as a wide-sense stationary process.

The analysis will concentrate on how the clutter characteristics vary across range cells. i.e., a quantified description of the change across range cells. We will identify how the observed clutter characteristics are subject to change due to the transmitted waveform, the manner in which the received signal is processed, platform motion, different shapes of antenna pattern, and system geometry. Finally, the analysis will cover both the monostatic and bistatic radar systems.

Chapter 2

Observation of Clutter Characteristics

In this chapter we will study how the clutter characteristics vary as a function of the system parameters, including the transmitted signal, pulse compression, radar platform motion, antenna pattern, and system geometry. The analysis starts with an examination of the clutter characteristics when observed from a stationary monostatic radar platform, and arrives at the generalized case where the radar platform is airborne and bistatic. The derivation is based on the point-scattering model, by which the clutter return is written as a linear superposition of the reflections from point scatterers. The secondary scattering effect is assumed to be negligible; the occurrence of the scatterers is then assumed to be governed by the spatial Poisson process.

2.1 Clutter observed from a stationary monostatic system

In the following we analyze the clutter characteristics when it is observed from a monostatic radar which is monostatic and is mounted on top of a stationary tower. The derivation is based on the point-scattering model where the clutter return is written as a linear superposition of the reflections from point scatterers distributed on the ground.

In this system, position of a point on the ground can be specified, relative to the radar site, by giving the height h of the platform and the azimuth angle φ and distance R of the

point. The projection of R on the ground is called the ground distance R_g,

$$R_g = \sqrt{R^2 - h^2}. \tag{2.1}$$

For convenience, we assume that the distance is measured in terms of the wave propagation time. The depression angle θ, measured from the local horizontal of the platform, positive downward, can be obtained from

$$\theta = \cos^{-1} \frac{R_g}{R}. \tag{2.2}$$

The scenario considered and the relationships of the parameters are illustrated in Figure 2.1.

The clutter return is assumed to be a linear superposition of the reflections from point scatterers distributed throughout the illuminated area. Denote by D_r the region swept by the transmitted pulse from the minimum to the maximum detection range. Using the subscript k to denote the quantities attributed to the kth scatterer, the total reflection from the scatterers in D_r can be written as

$$r_c(t) = \sum_{k=0}^{N_d} \frac{\tilde{g}_k}{R_k^2} G_T(\varphi_k, \theta_k) G_R(\varphi_k, \theta_k) s(t - 2R_k), \tag{2.3}$$

where N_d is the total number of scatterers in D_r. Let t_d be the signal round-trip travel time to some point in the range resolution cell D_c under consideration; also, denote the correlation operation by $\otimes$. The clutter return observed in D_c is given by

$$n_c(t_d) = \left\{ \sum_{k=0}^{N_d} \frac{g_k}{R_k^2} G_T(\varphi_k, \theta_k) G_R(\varphi_k, \theta_k) \tilde{s}(t - 2R_k) \right\} \otimes s(t - t_d). \tag{2.4}$$

Denoting the auto-correlation function of $s(t)$ by $\rho_s(\cdot)$,

$$\rho_s(\tau) = \int_{-\infty}^{\infty} s(t)s^*(t - \tau)dt, \tag{2.5}$$

the expression (2.4) can be written as

$$n_c(t_d) = \sum_{k=0}^{N_d} \frac{g_k}{R_k^2} G_T(\varphi_k, \theta_k) G_R(\varphi_k, \theta_k) \rho_s(t_d - 2R_k). \tag{2.6}$$

The clutter correlation is defined as

$$M_{n_c}(t_1, t_2) = E\left[n_c(t_1) n_c^*(t_2) \right]. \tag{2.7}$$
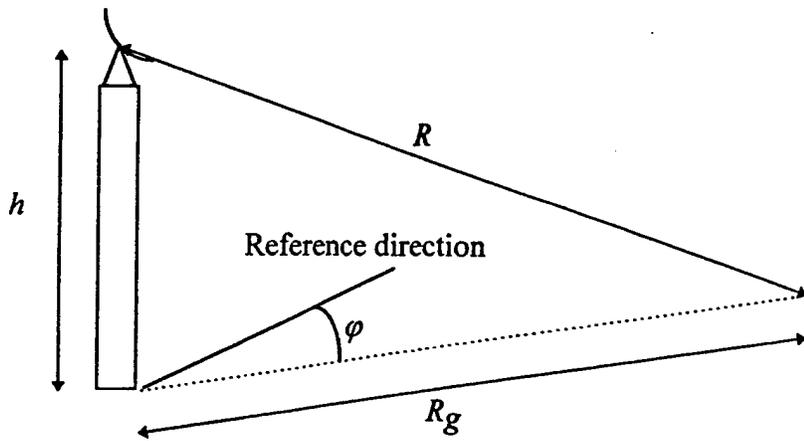
Figure 2.1: Geometry relationships for a stationary monostationary radar

The evaluation of (2.7) requires the joint probability distribution of the number, the location, and the reflectivity of the scatterers. For this purpose, we have the following assumptions. First, the occurrence of the scatterers is assumed to be governed by a spatial Poisson process [16],[17]. Due to the fact that an illuminated area usually consists of a number of regions having different scattering nature, e.g., patches of sand, vegetation, and artificial objects, we assume that the illuminated area can be divided into N_r such regions and the intensity function of the Poisson process, $\mu_c(R_g, \varphi)$, can be written as

$$\mu_c(R_g, \varphi) = \mu_{c,i} \quad \text{for } (R_g, \varphi) \in A_i, \ i = 1, \cdots, N_r, \tag{2.8}$$

where A_i is the ith region in D_r. It follows that the scatterers in each region are uniformly distributed when conditioned on a fixed number of scatterers [16], with the mean value $\mu_{c,i}|A_i|$, where $|A_i|$ is the size of A_i. Further, we assume that the scatterers are statistically independent of each other, the number of the scatterers is independent of the scatterer reflectivity and, in each A_i, there is a correlation function $\rho_{g,i}(\cdot)$ describing the fluctuation of the reflectivity of the scatterers, i.e.,

$$E[g_k(t_1)g_l^*(t_2)] = \rho_{g,i}(t_2 - t_1)\delta_{kl}, \tag{2.9}$$

for the kth and lth scatterers in A_i.

There is one more issue to be addressed before we can substitute (2.6) into (2.7) to evaluate the clutter correlation. The problem arises when the time axis of $n(t_1)$ and $n(t_2)$ has different origins. For example, this is the case when $n(t_1)$ and $n(t_2)$ are obtained from different pulses of a transmitted pulse train. Let the difference in time origins be T_d, with $n(t_2)$ having a later time origin. Then, denoting by D_φ and D_{R_g} the domains of the depression angle and the ground distance of the scatterers, respectively, and by N_c the number of A_i that fall within D_c, we have

$$M_{n_c}(t_1, t_2) = \sum_{i=1}^{N_A} \mu_{c,i}\rho_{g,i}(t_2 - t_1) \int_{D_{\varphi,i}} \int_{D_{R_g,i}} |G_T(\varphi, \theta)G_R(\varphi, \theta)|^2$$
$$\cdot \frac{1}{R^4}\rho_s(t_2 - T_d - 2R)\rho_s^*(t_1 - 2R)dR_g d\varphi. \tag{2.10}$$

12

In the above expression, the integration with respect to R_g can be changed to with respect to R by using (2.2), i.e.,

$$dR_g = \sec\theta dR. \tag{2.11}$$

Also. the integration interval D_c can be extended to infinity, since the product $\rho_s(t_2 - T_d - 2R)\rho_s^*(t_1 - 2R)$ is negligible outside of D_c; then,

$$M_{nc}(t_1, t_2) = \sum_{i=1}^{N_A} \mu_{c,i}\rho_{g,i}(t_2 - t_1) \int_{D_{\varphi,i}} \int_\infty^\infty |G_T(\varphi, \theta)G_R(\varphi, \theta)|^2$$
$$\cdot \frac{\sec\theta}{R^4}\rho_s(t_2 - T_d - 2R)\rho_s^*(t_1 - 2R)dRd\varphi. \tag{2.12}$$

Assume that the approximation of the factor $\sec\theta/R^4$ with a constant $\sec\theta_D/R_D^4$,

$$\theta_D = \cos^{-1}\frac{\sqrt{R_D^2 - h^2}}{R_D}, \tag{2.13}$$

within D_c does not result in appreciable error. Then,

$$M_{nc}(t_1, t_2) = \frac{\sec\theta_D}{R_D^4}\sum_{i=1}^{N_A} \mu_{c,i}\rho_{g,i}(t_2 - t_1) \int_{D_{\varphi,i}} \int_\infty^\infty |G_T(\varphi, \theta)G_R(\varphi, \theta)|^2$$
$$\cdot \rho_s(t_2 - T_d - 2R)\rho_s^*(t_1 - 2R)dRd\varphi. \tag{2.14}$$

Also. assume that the antenna patterns are approximately constant with respect to R within D_c. such that

$$|G_T(\varphi, \theta)| \cong |G_T(\varphi, \theta_D)| \tag{2.15}$$

and

$$|G_R(\varphi, \theta)| \cong |G_R(\varphi, \theta_D)|. \tag{2.16}$$

It follows that

$$M_{nc}(t_1, t_2) = \frac{\sec\theta_D}{R_D^4}\sum_{i=1}^{N_A} \mu_{c,i}\rho_{g,i}(t_2 - t_1) \int_{D_{\varphi,i}} |G_T(\varphi, \theta_D)G_R(\varphi, \theta_D)|^2$$
$$\cdot \int_\infty^\infty \rho_s(t_2 - T_d - 2R)\rho_s^*(t_1 - 2R)dRd\varphi. \tag{2.17}$$

Since the integral involving the two auto-correlation functions in (2.17) can be written as

$$\int_{-\infty}^\infty \rho_s(t_2 - T_d - 2R)\rho_s^*(t_1 - 2R)dR = 2\left\{\rho_s(t_2 - t_1 - T_d) \otimes \rho_s(t_2 - t_1 - T_d)\right\}, \tag{2.18}$$

13

we have

$$M_{n_c}(t_1, t_2) = \frac{\sec \theta_D}{2R_D^4} \sum_{i=1}^{N_A} \mu_{c,i} \rho_{g,i}(t_2 - t_1) \int_{D_{\varphi,i}} |G_T(\varphi, \theta_D) G_R(\varphi, \theta_D)|^2 \, d\varphi$$
$$\cdot \{\rho_s(t_2 - t_1 - T_d)\rho_s^*(t_2 - t_1 - T_d)\} \, . \tag{2.19}$$

The clutter power spectrum $\mathcal{M}_{n_c}(\cdot)$ is the Fourier transform of M_{n_c}. Denote the Fourier transforms of $\rho_g(\cdot)$ and $s(\cdot)$ by $\mathcal{P}_g(\cdot)$ and $S(\cdot)$, respectively. From the fact that

$$\int_{-\infty}^{\infty} \{\rho_s(x) \otimes \rho_s(x)\} \, e^{-j2\pi yx} dt = \left| \int_{-\infty}^{\infty} \rho_s(x) e^{-j2\pi yx} dt \right|^2 \tag{2.20}$$

and

$$\int_{-\infty}^{\infty} \rho_s(x) e^{-j2\pi yx} dx = |S(y)|^2 \, , \tag{2.21}$$

we have

$$\mathcal{M}_{n_c}(f) = \frac{\sec \theta_D}{2R_D^4} \sum_{i=1}^{N_A} \mu_{c,i} \left\{ \mathcal{P}_{g,i}(f) \otimes |S(f)|^4 \right\} \int_{D_{\varphi,i}} |G_T(\varphi, \theta_D) G_R(\varphi, \theta_D)|^2 \, d\varphi. \tag{2.22}$$

2.2 Clutter observed from an airborne monostatic system

In this section we generalize the previous analysis by assuming the radar platform is airborne. Through this examination, the effects of the relative motion between the radar platform and the illuminated scatterers on the observed clutter characteristics will be clear.

The relative motion between the radar platform and the scatterers induces Doppler shift ν. Explicitly, ν is a function of the platform speed v, the direction of v, the transmitted wavelength λ, and the location of the scatterer. Let (φ_v, θ_v) be the direction of v; then,

$$\nu = \frac{2v}{\lambda} \sin(\varphi - \varphi_v) \cos(\theta - \theta_v). \tag{2.23}$$

Comparing with (2.3), where the radar platform was assumed to be stationary, the reflections from the scatterers in D_r becomes

$$r_c(t) = \sum_{k=0}^{N_d} \frac{g_k}{R_k^2} G_T(\varphi_k, \theta_k) G_R(\varphi_k, \theta_k) s(t - 2R_k) e^{j2\pi \nu_k(t - 2R_k)} dR_g. \tag{2.24}$$

14

Suppose the return from range ring D_c is obtained by correlating the received signal with $s(t - t_d)\exp[j2\pi f_D(t - t_d)]$, where t_d is the travel time to some point in D_c and f_D is the Doppler shift with respect to a point in D_c. Consequently, the observed clutter return is given by

$$n_c(t_d) = \left\{ \sum_{k=0}^{N_d} \frac{g_k}{R_k^2} G_T(\varphi_k, \theta_k) G_R(\varphi_k, \theta_k) s(t - 2R_k) e^{j2\pi\nu_k(t-2R_k)} \right\} \otimes s(t - t_d) e^{j2\pi f_D(t-t_d)} \quad (2.25)$$

Denote the time-frequency correlation function of $s(t)$ by $\Phi_s(\cdot, \cdot)$,

$$\Phi_s(\tau, f) = \int_{-\infty}^{\infty} s\left(t + \frac{\tau}{2}\right) s^*\left(t - \frac{\tau}{2}\right) e^{-j2\pi ft} dt. \quad (2.26)$$

The expression (2.25) becomes

$$n_c(t_d) = \sum_{k=0}^{N_d} \frac{g_k}{R_k^2} G_T(\varphi_k, \theta_k) G_R(\varphi_k, \theta_k) \Phi_s(t_d - 2R_k, f_D - \nu_k) e^{j\pi(f_D-\nu_k)(t_d-2R_k)}. \quad (2.27)$$

With the same assumptions and procedures used in deriving (2.17), we have

$$M_{n_c}(t_1, t_2) = \frac{\sec\theta_D}{R_D^4} \sum_{i=1}^{N_A} \mu_{c,i} \rho_{g,i}(t_2 - t_1) \int_{D_{\varphi,i}} |G_T(\varphi, \theta_D) G_R(\varphi, \theta_D)|^2$$
$$\cdot \int_{\infty}^{\infty} \Phi_s(t_2 - T_d - 2R, f_D - \nu) \Phi_s^*(t_1 - 2R, f_D - \nu)$$
$$\cdot e^{j\pi(f_D-\nu)(t_2-t_1-T_d)} dR d\varphi. \quad (2.28)$$

Due to the dependence of ν on R, the right-hand side of (2.28) is not a function of $(t_2 - t_1)$ only: this indicates a non-stationary process. Then, it is of interest to find out if there are cases where the nonstationary effect is not significant.

Consider the effect of a small deviation $\triangle R$ of R_D on θ. The corresponding change of θ, $\triangle\theta$, can be found from the relationship

$$h = (R + \triangle R)\sin(\theta + \triangle\theta) = R\sin\theta. \quad (2.29)$$

Using the small angle approximation

$$\sin\triangle\theta \cong \triangle\theta \quad (2.30)$$

and straightforward manipulation of (2.29), we have

$$\triangle\theta = \tan\theta \frac{-\triangle R/R}{1 + \triangle R/R}. \quad (2.31)$$

15

In practice, it is usually true that the width of the range ring is much smaller than the minimum detection range; in other words, $\triangle R/R \ll 1$, for all R. Thus,

$$\triangle\theta = \tan\theta\frac{-\triangle R}{R}. \qquad (2.32)$$

With the approximation

$$\cos\triangle\theta \cong 1, \qquad (2.33)$$

the value of the cosine factor around $(\theta_D - \theta_v)$ can be written as

$$\cos(\theta_D + \triangle\theta - \theta_v) = \cos(\theta_D - \theta_v) - \sin(\theta_D - \theta_v)\triangle\theta. \qquad (2.34)$$

From (2.23), (2.32) and (2.34), the Doppler shift in the reflections from the scatterers located near R_D can be approximated by

$$\nu = \frac{2v}{\lambda}\sin(\varphi - \varphi_v)\cos(\theta_D - \theta_v) + \frac{2v}{\lambda}\sin(\varphi - \varphi_v)\sin(\theta_D - \theta_v)\tan\theta_D\frac{\triangle R}{R_D}. \qquad (2.35)$$

It can be seen from (2.35) that, by denoting the first term on the right-hand side by ν_D and the second term by $\triangle\nu$; the quantity $\triangle\nu$ can be ignored when

$$\frac{\sin(\theta_D - \theta_v)\tan\theta_D\triangle R/R_D}{\cos(\theta_D - \theta_v)} = \tan(\theta_D - \theta_v)\tan\theta_D\frac{\triangle R}{R_D} \ll 1. \qquad (2.36)$$

Therefore, it is sufficient that

$$\tan(\theta_D - \theta_v)\tan\theta_D < 1 \qquad (2.37)$$

for (2.36) to be true, e.g., $\theta_D < \pi/4$ is sufficient when $\theta_v = 0$. The clutter correlation (2.28) becomes

$$M_{n_c}(t_1, t_2) = \frac{\sec\theta_D}{R_D^4}\sum_{i=1}^{N_A}\mu_{c,i}\rho_{g,i}(t_2 - t_1)$$
$$\cdot\int_{D_{\varphi,i}}|G_T(\varphi, \theta_D)G_R(\varphi, \theta_D)|^2\,e^{j\pi(f_D - \nu_D)(t_2 - t_1 - T_d)}$$
$$\cdot\int_\infty^\infty \Phi_s(t_2 - T_d - 2R, f_D - \nu)\Phi_s^*(t_1 - 2R, f_D - \nu) \qquad (2.38)$$

In the rest of this analysis, we consider only the case where $\triangle\nu \ll \nu_D$.

16

In a manner similar to the derivation of (2.19), we have

$$
\begin{aligned}
M_{n_c}(t_1, t_2) =\ & \frac{\sec \theta_D}{R_D^4} \sum_{i=1}^{N_A} \mu_{c,i} \rho_{g,i}(t_2 - t_1) \\
& \cdot \int_{D_{\varphi,i}} |G_T(\varphi, \theta_D) G_R(\varphi, \theta_D)|^2\, e^{j\pi(f_D - \nu_D)(t_2 - t_1 - T_d)} \\
& \cdot \{\Phi_s(t_2 - t_1 - T_d, f_D - \nu)\Phi_s^*(t_2 - t_1 - T_d, f_D - \nu)\}\, d\varphi. \quad (2.39)
\end{aligned}
$$

The clutter power spectrum is readily obtained by taking the Fourier transform of the right-hand side of (2.39). From the fact that

$$
\int_{-\infty}^{\infty} \{\Phi_s(x, y) \otimes \Phi_s(x. y)\}\, e^{-j2\pi w x}\, dx = \left| \int_{-\infty}^{\infty} \Phi_s(x, y) \right|^2. \quad (2.40)
$$

and

$$
\int_{-\infty}^{\infty} \Phi_s(x, y) e^{-j2\pi w x}\, dx = S\left(w + \frac{y}{2}\right) S^*\left(w - \frac{y}{2}\right), \quad (2.41)
$$

we have

$$
\begin{aligned}
\mathcal{M}_{n_c}(f) =\ & \frac{\sec \theta_D}{R_D^4} \sum_{i=1}^{N_A} \mu_{c,i} \int_{D_{\varphi,i}} |G_T(\varphi, \theta_D) G_R(\varphi, \theta_D)|^2 \\
& \cdot \left\{ \mathcal{P}_{g,i}\left(f - \frac{f_D - \nu_D}{2}\right) \otimes |S(f) S(f - (f_D - \nu_D))|^2 \right\} d\varphi. \quad (2.42)
\end{aligned}
$$

2.3 Clutter observed from an airborne bistatic system

In the following we consider the case where the radar platform is airborne and bistatic. The effects of geometry on clutter will be examined in detail.

The Cartesian coordinate system is used to describe the three dimensional bistatic geometry. Let the transmitter site be the origin; this choice is arbitrary and will be discussed later. Let the local horizontal plane of the transmitter be the x-y plane. The vertical line passing through the transmitter is chosen to be the z-axis, and the intersection of the x-y plane and the vertical plane containing the transmitter and the receiver is chosen to be the x-axis; y-axis is defined according to the right-hand rule. Further, assume that the depression angle is measured from the x-y plane, positive downward, and the azimuth angle is measured from y-axis, positive clockwise.

For simplicity of expression, measurements relative both to the transmitter and to the receiver are used. In particular, we assume that the angle measurements relative to the receiver are obtained by translating the origin from the the transmitter site to the receiver site. The same symbols for the angle and distance measurements used in the monostatic case are kept for the present analysis; however, subscripts T and R are added to indicate that the quantity is measured relative to the transmitter or the receiver. For example, R_T is the distance of a point from the transmitter and R_{T_g} is the ground projection of R_T.

$$R_{T_g} = \sqrt{R_T^2 - h_T^2} \tag{2.43}$$

The symbol R is now used to denote the total distance the signal traveled: $R = R_T + R_R$. Finally, let L denote the distance between the transmitter and the receiver. The scenario considered, together with the relationships of the parameters, is illustrated in Figure 2-2. Specifically, the quantities R_R, φ_R and θ_R can be expressed as functions of R_T, φ_T and θ_T by knowing the relative positions between the transmitter and the receiver. Let depression angles of the receiver with respective to the transmitter be θ_{RT}; clearly, the azimuth angle of the receiver relative to the transmitter is $\pi/2$. From the law of cosines,

$$R_R = \left[R_{T_g}^2 + L^2 \cos^2 \theta_{RT} - 2R_{T_g}L \cos\theta_{RT} \sin\varphi_T + h_R^2 \right]^{1/2}. \tag{2.44}$$

Using the relationships

$$R_T \sin\theta_T = R_R \sin\theta_R + L \sin\theta_{RT} \tag{2.45}$$

and

$$R_T \cos\varphi_T \cos\theta_T = R_R \cos\varphi_R \cos\theta_R, \tag{2.46}$$

it can be shown that

$$\theta_R = \sin^{-1}\left[(R_T \sin\theta_T - L \sin\theta_{RT})/R_R \right] \tag{2.47}$$

and

$$\varphi_R = \cos^{-1}\left\{ (R_T \cos\varphi_T \cos\theta_T \left[R_T^2 \cos^2\theta_T + L^2 \cos^2\theta_{RT} \right.\right.$$
$$\left.\left. \cdot +2R_T L \cos\theta_T \cos\theta_{RT} \cos(\varphi_T - \varphi_{RT})\right]^{-1/2} \right\}. \tag{2.48}$$

18
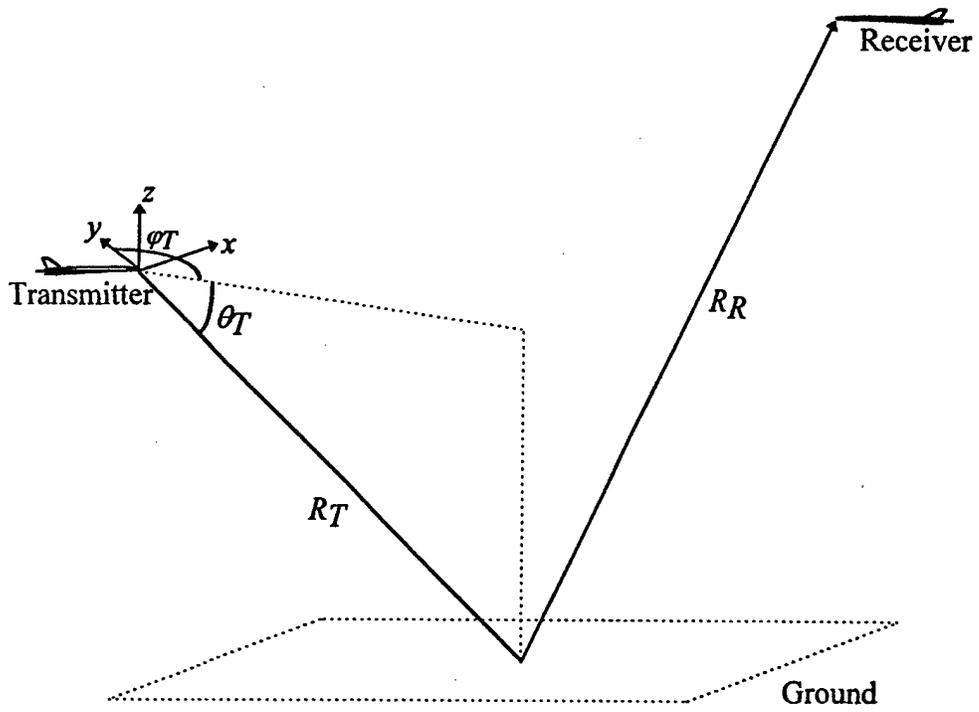
Figure 2.2: Geometry relationships for the airborne bistatic radar

In comparison with the clutter model (2.25), the factor R^{-2} representing the propagation loss becomes $(R_T R_R)^{-1}$. Also, the Doppler shift depends on the bistatic geometry. Let the transmitter's speed relative to the ground be v_T, in the direction $(\varphi_{v_T}, \theta_{v_T})$, and the receiver's speed relative to the ground be v_R, in the direction $(\varphi_{v_R}, \theta_{v_R})$. The resulting Doppler shift is given by

$$\nu = \frac{v_T}{\lambda} \sin(\varphi_T - \varphi_{v_T}) \cos(\theta_T - \theta_{v_T}) + \frac{v_R}{\lambda} \sin(\varphi_R - \varphi_{v_R}) \cos(\theta_R - \theta_{v_R}). \tag{2.49}$$

Hence. the clutter return is written as

$$n_c(t) = \left\{ \sum_{k=0}^{N_d} \frac{g_k}{R_{T_k} R_{R_k}} G_T(\varphi_{T_k}, \theta_{T_k}) G_R(\varphi_{R_k}, \theta_{R_k}) s(t - R_k) e^{j2\pi\nu_k(t-R_k)} \right\}$$
$$\otimes s(t - t_D) e^{j2\pi f_D(t-t_D)} \tag{2.50}$$

Then, similar to the monostatic case, we assume that the reflectivity of the scatterers are statistically independent from the number and from the location of the scatterers, and the occurrence of the scatterers is governed by the non-homogeneous spatial Poisson process. The bistatic clutter correlation function becomes

$$M_{n_c}(t_1, t_2) = \sum_{i=1}^{N_A} \mu_{c,i} \rho_{g,i}(t_2 - t_1) \int_{D_{\varphi_T,i}} \int_{-\infty}^{\infty} |G_T(\varphi_T, \theta_T) G_R(\varphi_R, \theta_R)|^2 \frac{1}{(R_T R_R)^2}$$
$$\cdot \Phi_s(t_2 - T_d - R, f_D - \nu) \Phi_s^*(t_1 - R, f_D - \nu)$$
$$\cdot e^{j\pi(f_D-\nu)(t_2-t_1-T_d)} dR_{T_g} d\varphi_T. \tag{2.51}$$

It should be noted that, in (2.51), the integration over R_{T_g} is due to the choice of the transmitter site as the origin of the coordinate system; the integration over R_{T_g} can be changed to over R. Define the factors

$$A = L \cos \theta_{RT} \sin \varphi_T \tag{2.52}$$

and

$$B = h_T^2 - h_R^2 - L^2 \cos^2 \theta_{RT}. \tag{2.53}$$

Using the fact that $R_R = R - R_T$ and the relationship (2.44), it can be shown that

$$R_{T_g} = \left[A(R^2 + B) + R\sqrt{(R^2 + B)^2 - 4h_T^2(R^2 - A^2)} \right] \Big/ \left[2(R^2 - A^2) \right], \tag{2.54}$$

20

for $R \geq h_T + \sqrt{L^2 \cos^2 \theta_{RT} + h_R^2}$, and

$$R_{T_g} = \left[A(R^2 + B) \pm R\sqrt{(R^2 + B)^2 - 4h_T^2(R^2 - A^2)} \right] \Big/ \left[2(R^2 - A^2) \right]. \qquad (2.55)$$

We have the following observation for the case $R < h_T + \sqrt{L^2 \cos^2 \theta_{RT} + h_R^2}$. The region $R < h_T - \sqrt{L^2 \cos^2 \theta_{RT} + h_R^2}$ on the ground is inside the contour defined by the intersection of the ellipsoid $R = h_T + \sqrt{L^2 \cos^2 \theta_{RT} + h_R^2}$ and the ground. When the region $R < h_T + \sqrt{L^2 \cos^2 \theta_{RT} + h_R^2}$ is larger than $R \geq h_R + \sqrt{L^2 \cos^2 \theta_{RT} + h_T^2}$, it is more convenient to set the origin of the coordinate system at the receiver instead of the transmitter. In such regions, there are two intersections with the constant range contour in the transmitter's line of sight and may result in ambiguities; we only consider the case where $R \geq h_T + \sqrt{L^2 \cos^2 \theta_{RT} + h_R^2}$. The analysis can easily be extended to the case where $R < h_T + \sqrt{L^2 \cos^2 \theta_{RT} + h_R^2}$ by adding the additional clutter return. It can be shown that

$$\frac{dR_{T_g}}{dR} = 2R_T R_R \left[(R^2 + B)^2 - 4h_T^2(R^2 - A^2) \right]^{-1/2}. \qquad (2.56)$$

More discussions on R_T, R_R and R_{T_g} are given in Appendix A.

From the foregoing derivation, the clutter correlation function (2.51) can be written as

$$M_{n_c}(t_1, t_2) = \sum_{i=1}^{N_A} \mu_{c,i} \rho_{g,i}(t_2 - t_1) \int_{D_{\varphi_T,i}} \int_{-\infty}^{\infty} |G_T(\varphi_T, \theta_T) G_R(\varphi_R, \theta_R)|^2$$
$$\cdot \frac{1}{(R_T R_R)^2} \Phi_s(t_2 - T_d - R, f_D - \nu) \Phi_s^*(t_1 - R, f_D - \nu) e^{j\pi(f_D - \nu)(t_2 - t_1 - T_d)}$$
$$\cdot 2R_T R_R \left[(R^2 + B)^2 - 4h_T^2(R^2 - A^2) \right]^{-1/2} dR d\varphi_T. \qquad (2.57)$$

For simplicity of notation, define the quantity

$$Q = 2R_T R_R \left[(R^2 + B)^2 - 4h_T^2(R^2 - A^2) \right]^{-1/2}. \qquad (2.58)$$

Thus,

$$M_{n_c}(t_1, t_2) = \sum_{i=1}^{N_A} \mu_{c,i} \rho_{g,i}(t_2 - t_1) \int_{D_{\varphi_T,i}} \int_{-\infty}^{\infty} |G_T(\varphi_T, \theta_T) G_R(\varphi_R, \theta_R)|^2 \frac{Q}{(R_T R_R)^2}$$
$$\cdot \Phi_s(t_2 - T_d - R, f_D - \nu) \Phi_s^*(t_1 - R, f_D - \nu) e^{j\pi(f_D - \nu)(t_2 - t_1 - T_d)} dR d\varphi_T \qquad (2.59)$$

Suppose D_c is short enough that a constant R_D can be used in calculating the factor $Q/(R_T R_R)^2$ without causing appreciable error. Let R_{T_D}, R_{R_D} and Q_D denote the quantities

21

obtained by substituting R_D into (A.1) and (A.3) of Appendix A and (2.58), respectively, e.g..

$$Q_D = 2R_{T_D}R_{R_D} \left[(R_D^2 + B)^2 - 4h_T^2(R_D^2 - A^2)\right]^{-1/2}.$$ (2.60)

Then.

$$M_{n_c}(t_1, t_2) = \sum_{i=1}^{N_A} \mu_{c,i}\rho_{g,i}(t_2 - t_1)\int_{D_{\varphi T,i}} \frac{Q_D}{(R_{T_D}R_{R_D})^2}\int_{-\infty}^{\infty} |G_T(\varphi_T, \theta_T)G_R(\varphi_R, \theta_R)|^2$$
$$\cdot\Phi_s(t_2 - T_d - R, f_D - \nu)\Phi_s^*(t_1 - R, f_D - \nu)\epsilon^{j\pi(f_D-\nu)(t_2-t_1-T_d)}dRd\varphi_T \quad (2.61)$$

Similar to the monostatic case, we assume that the antenna patterns are insensitive to the change of R within D_c; let θ_{T_D} and θ_{R_D} denote the depression angles evaluated at a constant R_D in D_c, e.g..

$$\theta_{T_D} = \sin^{-1}\frac{h_T}{R_{T_D}}.$$ (2.62)

It follows that

$$M_{n_c}(t_1, t_2) = \sum_{i=1}^{N_A} \mu_{c,i}\rho_{g,i}(t_2 - t_1)\int_{D_{\varphi T,i}} \frac{Q_D}{(R_{T_D}R_{R_D})^2} |G_T(\varphi_T, \theta_T)G_R(\varphi_R, \theta_R)|^2$$
$$\cdot\int_{-\infty}^{\infty} \Phi_s(t_2 - T_d - R, f_D - \nu)\Phi_s^*(t_1 - R, f_D - \nu)$$
$$\cdot\epsilon^{j\pi(f_D-\nu)(t_2-t_1-T_d)}dRd\varphi_T.$$ (2.63)

The expression (2.63) indicates a nonstationary process since ν varies with R such that (2.63) is not a function of $(t_2 - t_1)$. The condition under which the Doppler shift can be considered approximately constant with respect to R within one range ring was analyzed for the monostatic case; the derivation can be extended to the bistatic case. It can be seen from the derivation of (2.31) to (2.36) that it is sufficient to have

$$\tan(\theta_{T_D} - \theta_{v_T})\tan\theta_{T_D}\frac{\triangle R_T/R_{T_D}}{1 + \triangle R_T/R_{T_D}} \ll 1$$ (2.64)

and

$$\tan(\theta_{R_D} - \theta_{v_R})\tan\theta_{R_D}\frac{\triangle R_R/R_{R_D}}{1 + \triangle R_R/R_{R_D}} \ll 1.$$ (2.65)

For ν to be insensitive to the change of R in one range ring consider the factors $\triangle R_T/R_{T_D}$ and $\triangle R_R/R_{R_D}$. It is expected that those two factors are also much less than unity when

$\triangle R/R \ll 1$ for one range ring for fairly general geometry. The change of R_T due to a small change of R is governed by the differentiation of R_T with respect to R. Using chain rule, we have

$$\frac{dR_T}{dR} = \frac{dR_T}{dR_{T_g}}\frac{dR_{T_g}}{dR}. \tag{2.66}$$

From (2.43) and (2.56), we have

$$\frac{dR_T}{dR} = 2R_{T_g}R_R \left[(R^2 + B)^2 - 4h_T^2(R^2 - A^2)\right]^{-1/2}. \tag{2.67}$$

It follows that

$$\frac{dR_T}{R_T} = 2\frac{R_{T_g}}{R_T}R_R \left[(R^2 + B)^2 - 4h_T^2(R^2 - A^2)\right]^{-1/2} dR. \tag{2.68}$$

Substituting (A.3) from Appendix A for R_R, we have

$$\frac{dR_T}{R_T} = \frac{R_{T_g}}{R_T} \left[\frac{1 - 2A^2/R^2 - B/R^2}{(1 - A^2/R^2)\sqrt{(1 + B/R^2)^2 - 4h_T^2/R^2(1 - A^2/R^2)}} - \frac{A/R}{1 - A^2/R^2}\right] \frac{dR}{R}. \tag{2.69}$$

Assume that the square of the ratios h_T/R, h_R/R and L/R are much smaller than unity; it follows that A^2/R^2 and B/R^2 are negligible compared to unity and R_{T_g}/R_T is close to unity. Consequently,

$$\frac{dR_T}{R_T} = \left(1 - \frac{A}{R}\right)\frac{dR}{R}. \tag{2.70}$$

From the definition of A given by (2.52), we have $|A/R| < 1$. Then, we conclude from (2.70) that $\triangle R_T/R_T \ll 1$ when $\triangle R/R \ll 1$ within one range ring. The analysis of the condition for $\triangle R_{R_g}/R_R$ to be much smaller than unity follows similar procedure as that for $\triangle R_{T_g}/R_T$: it is given in Appendix A.

The factors $|\tan\theta_{T_D}|$ and $|\tan\theta_{R_D}|$ are smaller than unity by the previous assumptions; therefore, it is sufficient to have $|\tan(\theta_{T_D} - \theta_{v_T})|$ and $|\tan(\theta_{T_D} - \theta_{v_T})|$ to be smaller than unity for (2.64) and (2.65) to be true. Assume that $|\tan(\theta_{T_D} - \theta_{v_T})|$ and $|\tan(\theta_{T_D} - \theta_{v_T})|$ are smaller than unity in the analysis to follow. Let ν_D denote the quantity

$$\nu_D = \frac{v_T}{\lambda}\sin(\varphi_T - \varphi_{v_T})\cos(\theta_{T_D} - \theta_{v_T}) + \frac{v_R}{\lambda}\sin(\varphi_R - \varphi_{v_R})\cos(\theta_{R_D} - \theta_{v_R}). \tag{2.71}$$

With the above analysis, it is seen that ν is insensitive to the change of R within one range ring when the assumptions are true, such that

$$M_{n_c}(t_1, t_2) = \sum_{i=1}^{N_A} \mu_{c,i}\rho_{g,i}(t_2 - t_1) \int_{D_{\varphi_T,i}} \frac{Q_D}{(R_{T_D}R_{R_D})^2} |G_T(\varphi_T, \theta_{T_D})G_R(\varphi_R, \theta_{R_D})|^2$$

$$\cdot \left\{ \Phi_s(t_2 - t_1 - T_d. f_D - \nu_D) \otimes \Phi_s^*(t_2 - t_1 - T_d, f_D - \nu_D) \right\}$$

$$\cdot e^{j\pi(f_D - \nu_D)(t_2 - t_1 - T_d)} d\varphi_T. \tag{2.72}$$

It follows that

$$\mathcal{M}_{n_c}(f) = \sum_{i=1}^{N_A} \mu_{c,i} \int_{D_{\varphi_T,i}} \left\{ \mathcal{P}_{g,i} \left(f - \frac{f_D - \nu_D}{2} \right) \otimes |S(f)S(f - (f_D - \nu_D))|^2 \right\}$$

$$\cdot \frac{Q_D}{(R_{T_D} R_{R_D})^2} |G_T(\varphi_T, \theta_{T_D}) G_R(\varphi_R, \theta_{R_D})|^2 d\varphi_T \tag{2.73}$$

2.4 Detection of target in clutter

The effects of ground clutter return on the detection performance in both the space-time and time domain processing are considered in the follwoing. In particular, we examine the SCNR at the receiver output. This quantity is also proportional to the detection probability in the Gaussian interference case.

The receiver output SCNR was given by (1.1), and its maximum is attained by using the weights specified by (1.2). As a result.

$$d^2 = s^H R_n^{-1} s. \tag{2.74}$$

Suppose that the thermal noise has power σ_n^2 and denote the clutter covariance matrix by R_c: the expression (2.74) becomes

$$d^2 = s^H \left(\sigma_n^2 I + R_c \right)^{-1} s, \tag{2.75}$$

where I denotes the identity matrix and R_c denotes the clutter correlation matrix. Specifically, R_n can be written as

$$R_n = \begin{bmatrix} \sigma_n^2 I + R_{c_0} & R_{c_1} & \cdots & R_{c_{N-1}} \\ R_{c_1}^* & \sigma_n^2 I + R_{c_0}^* & & \\ \vdots & & \ddots & \\ R_{c_{N-1}}^* & & & \sigma_n^2 I + R_{c_0} \end{bmatrix}, \tag{2.76}$$

where each R_{c_i} is the correlation matrix due to the clutter component of the output of the array sensors at i pulses apart, and N is the number of the received pulses. In other words,

the (k, l)th element of R_{c_i} is given by $E[n_{c_k}(t)n_{c_l}^*(t - iT)]$. It follows that R_n is not of full rank if $\sigma_n = 0$ and $E[s_k(t)s_l^*(t - iT)] = E[s_p(t)s_q^*(t - iT)]$. When this problem arises, it can be avoided by adding a small quantity to the diagnal of R_n. In the following, without making further assumptions regarding the observed clutter characteristics across the array sensors, we will only consider the SCNR at the output of a single sensor on a bistatic receiver. A more thorough investigation of the utility of (2.39) and (2.72), especially in the context of space-time processing, is the focus of the continuing effort.

The derivation of the SCNR at the output of a single sensor receiver is discussed in detail in [3]:

$$\text{SCNR} = \int_{-\infty}^{\infty} \frac{|S_d(f)|^2}{\sigma_n^2 + \mathcal{M}_{n_c}^*(f)} df, \tag{2.77}$$

where $S_d(f)$ is the desired signal from the receiver output.

The result (2.77) has two important consequences. First, it can be seen that the performance of the optimum receiver is the same as the matched filter when $\mathcal{M}_{n_c}^*(f)$ is displaced from $S_d(f)$. Therefore, it indicates that the receiver structure can be simplified with properly designed transmitted signal. This subject was studied in detail in the literature, e.g. [5]; however, no consideration has been given in the context of space-time processing.

The second issue associated with (2.77) is when $S(f)$ is wide but $\mathcal{P}_g^*(f)$ is narrow, in terms of the quantity $f_D - \nu_D$, i.e., the Doppler spread in one resolution cell. If we can further assume that the illuminated ground clutter is homogeneous, it can be seen from (2.73) that the area of the resolution cell becomes the dominant factor which affects the receiver output SCNR. Specifically, when the the illuminated ground clutter is homogeneous, we can write

$$\mathcal{M}_{n_c}(f) = \mu_c \int_{D_{\varphi_T}} \left\{ \mathcal{P}_g \left(f - \frac{f_D - \nu_D}{2} \right) \otimes |S(f)S(f - (f_D - \nu_D))|^2 \right\}$$
$$\cdot \frac{Q_D}{(R_{T_D} R_{R_D})^2} |G_T(\varphi_T, \theta_{T_D}) G_R(\varphi_R, \theta_{R_D})|^2 d\varphi_T \tag{2.78}$$

From the above expression it is seen that, by letting an impulse function to approximate $\mathcal{P}_g^*(f)$ and letting a constant to approximate $S(f)$ in the correlation calculation, the integral is affected by the geometry factors alone. In the following we give an example to illustrate this observation.

25

Example

In this example we we consider the clutter return in a bistatic system where both the transmitter and the receiver depression angles are small. We assume that the transmit beam is omnidirectional but the receive beam is narrow with a 3 dB beamwidth of 2 deg; for simplicity, we further assume that the receive beam pattern is uniform within the 3 dB beamwidth and negligible elsewhere. The above assumption about the receive beam is one of the two models which are generally adopted in the literature, while Gaussian beam pattern is the other one. Thus, we have

$$\int_{D_{\varphi_T}} \frac{Q_D}{(R_{T_D} R_{R_D})^2} |G_T(\varphi_T, \theta_{T_D}) G_R(\varphi_R, \theta_{R_D})|^2 \, d\varphi_T = \int_{D_B} \frac{Q_D}{(R_{T_D} R_{R_D})^2} d\varphi_T, \qquad (2.79)$$

where D_B is the ground intersection of the beam and the distance corresponding to one range cell. The quantity on the right-hand side of (2.79) is evaluated along three range rings, at the receiver look angle from $-\pi$ to π, while each range ring is specified in terms of its eccentricity e, $R = L/e$. Figure 2.3 shows the geometry of $e = 0.4$ by having the baseline to be 50km and the range ring, the inner circle in the plot, to be 125km. The results are plotted by normalizing with respect to the value obtained at $\varphi_R = \pi/2$. Thus, the plots can be used for any geometry irregardless of the actual values of R and L. Figures 2.4 to 2.6 give the results for $e = 0.4$, $e = 0.1$ and $e = 0.025$, respectively.

From these figures it is seen that the geometry factors have mild to minimal effects on the clutter power. This conclusion is consistent with results in the literature where the change of illuminated area is considered to be the dominant factor in the variation of the clutter power. However, it should be emphasized that the applicability of the results shown in this example relies on the vailidity of the simplification that leads to (2.79).
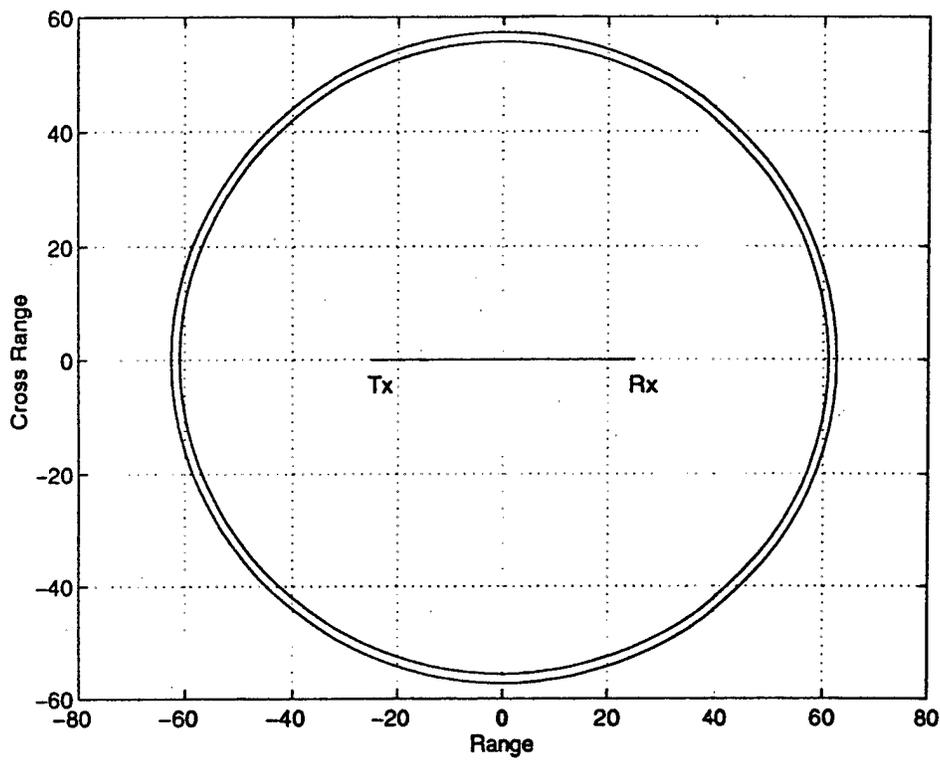
Figure 2.3: Isorange Contour at eccentricity of 0.4
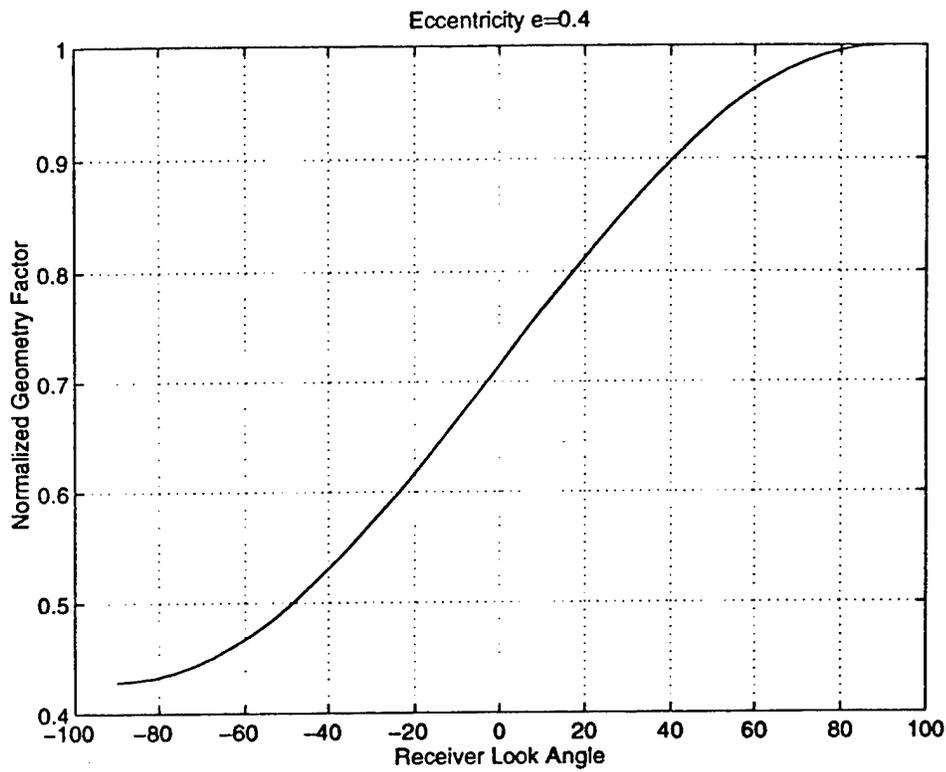
Figure 2.4: Normalized geometry factor at eccentricity of 0.4
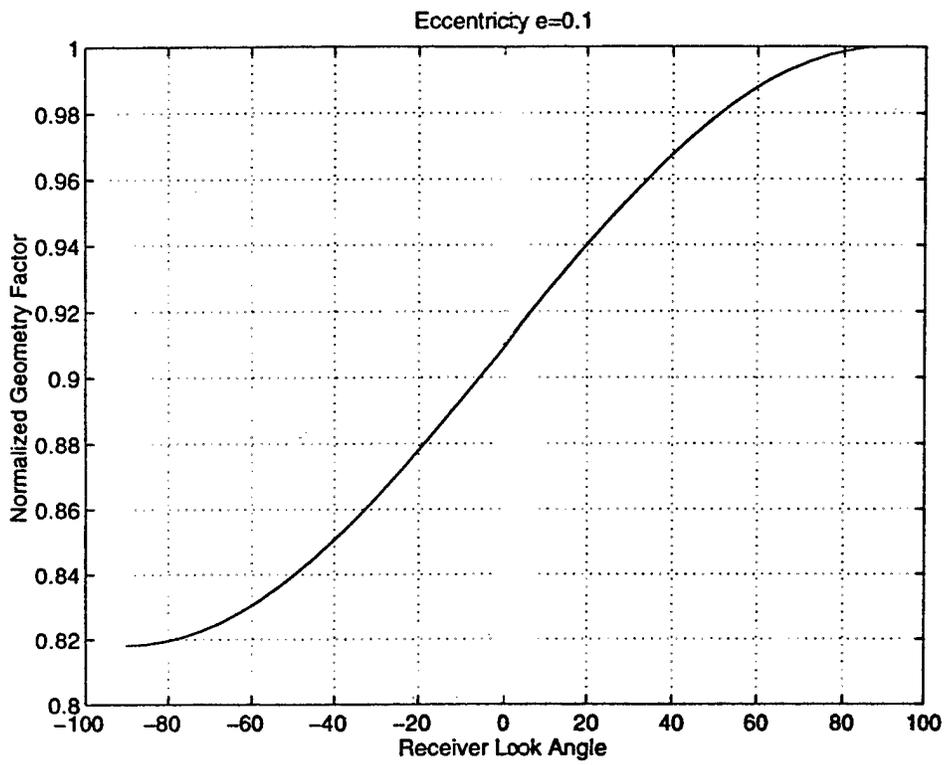
Figure 2.5: Normalized geometry factor at eccentricity of 0.1
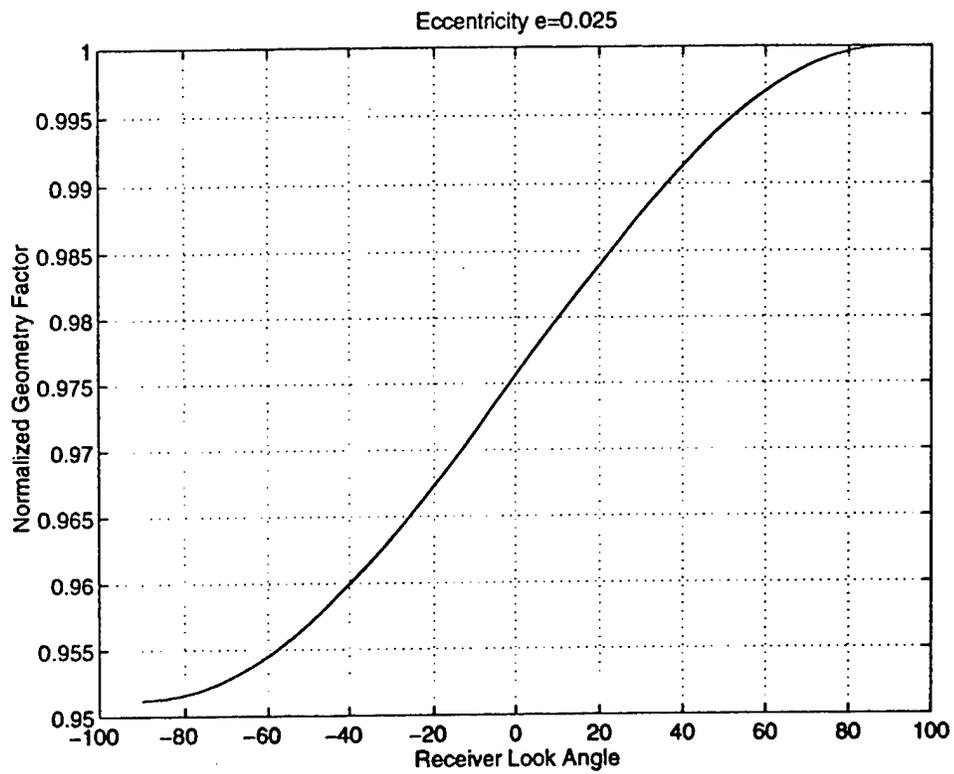
Figure 2.6: Normalized geometry factor at eccentricity of 0.025

Chapter 3

Doppler Spread of the Ground Clutter in Airborne Bistatic Radar

This chapter concerns the Doppler spread of the ground clutter in airborne bistatic radars. The subject of Doppler spread of the clutter in the bistatic plane was treated in [16]. Here we extend the development to three-dimension, assuming flat earth. This assumption is useful when the illuminated region on the ground is small such that it can be approximated by a plane. To facilitate the analysis, we first derive some results on the three-dimensional bistatic geometry. The ground clutter Doppler spread is studied in Section 2.

3.1   Constant range and constant Doppler contours

In this section, we show how the intersection of the constant range contour and the ground can be described for an airborne bistatic radar, with the assumption of flat earth. The illuminated portion of this intersection gives the cross-range dimension of the resolution cell on the ground.

Expressed in terms of the Cartesian coordinate system, the constant range contour in an airborne bistatic radar is an ellipsoid given by

$$\left(x^2 + y^2 + z^2\right)^{1/2} + \left[(x - L\cos\theta_{RT})^2 + y^2 + (z - h_R + h_T)^2\right]^{1/2} = R. \tag{3.1}$$

Assuming flat earth, the intersection of this ellipsoid with the ground is an ellipse, which can be found by setting $z = -h_T$ in (3.1). With this substitution and straightforward algebraic

manipulations, the expression for the ellipse is obtained as

$$\frac{(x-d)^2}{a^2} + \frac{y^2}{b^2} = 1,$$ (3.2)

where the major axis is

$$a = \frac{R}{2}\left[1 - \frac{(h_R - h_T)^2}{R^2 - L^2\cos^2\theta_{RT}}\right]^{1/2}\left[1 - \frac{(h_R + h_T)^2}{R^2 - L^2\cos^2\theta_{RT}}\right]^{1/2},$$ (3.3)

the minor axis is

$$b = \frac{(R^2 - L^2\cos^2\theta_{RT})^{1/2}}{2}\left[1 - \frac{(h_R - h_T)^2}{R^2 - L^2\cos^2\theta_{RT}}\right]^{1/2}\left[1 - \frac{(h_R + h_T)^2}{R^2 - L^2\cos^2\theta_{RT}}\right]^{1/2},$$ (3.4)

the translation in the x-axis is

$$d = \frac{L\cos\theta_{RT}}{2}\left(1 - \frac{h_R^2 - h_T^2}{R^2 - L^2\cos^2\theta_{RT}}\right),$$ (3.5)

and $sqrt{R^2 - L^2\cos^2\theta_{RT}} \geq (h_R + h_T)$ is assumed to insure that the intersection exists. Using the definition $c = \sqrt{a^2 - b^2}$, the location of the foci of the ellipse can be written as $(-c + d, 0, -h_T)$ and $(c + d, 0, -h_T)$.

To determine the extent of a range cell, the coordinate of the points on the contour (3.2) as function of the transmitter or receiver azimuth angle is needed. Clearly, the points on the ground at a given φ_T satisfy $y = \tan\varphi_T x$. Substituting this relationship into (3.2), we obtain the coordinates

$$x = \frac{b^2 d\cos^2\varphi_T + ab\cos\varphi_T\sqrt{(a^2 - d^2)\sin^2\varphi_T + b^2\cos^2\varphi_T}}{a^2\sin^2\varphi_T + b^2\cos^2\varphi_T}$$ (3.6)

and

$$y = \frac{b^2 d\sin\varphi_T\cos\varphi_T + ab\tan\varphi_T\cos\varphi_T\sqrt{(a^2 - d^2)\sin^2\varphi_T + b^2\cos^2\varphi_T}}{a^2\sin^2\varphi_T + b^2\cos^2\varphi_T},$$ (3.7)

where the condition that $|\varphi_T| \leq \tan^{-1}(b/\sqrt{d^2 - a^2})$, when $d > a$, and $\pi - \tan^{-1}(b/\sqrt{d^2 - a^2}) \leq \varphi_T \leq \pi + \tan^{-1}(b/\sqrt{d^2 - a^2})$, when $d < -a$, is imposed to insure the intersection exists. Similarly, the intersection of the receiver line-of-sight with (3.2) can be obtained by substituting $y = \tan\varphi_R(x - L_g)$ into (3.2); thus, we have

$$x = \frac{a^2 L_g\sin^2\varphi_R + b^2 d\cos^2\varphi_R + ab\cos\varphi_R\sqrt{[a^2 - (d - L_g)^2]\sin^2\varphi_R + b^2\cos^2\varphi_R}}{a^2\sin^2\varphi_R + b^2\cos^2\varphi_R}$$ (3.8)

32

and

$$y = \frac{b^2(d - L_g)\sin\varphi_R\cos\varphi_R + ab\tan\varphi_R\cos\varphi_R\sqrt{[a^2 - (d - L_g)^2]\sin^2\varphi_R + b^2\cos^2\varphi_R}}{a^2\sin^2\varphi_R + b^2\cos^2\varphi_R}, \quad (3.9)$$

where the condition that $|\varphi_R| \leq \tan^{-1}(b/\sqrt{(d - L_g)^2 - a^2})$, when $(d - L_g) > a$, and $\pi - \tan^{-1}(b/\sqrt{(d - L_g)^2 - a^2}) \leq \varphi_T \leq \pi + \tan^{-1}(b/\sqrt{(d - L_g)^2 - a^2})$, when $(d - L_g) < -a$, is imposed to insure the intersection exists.

The derivations in this section are based on the assumption of flat earth. This assumption is applicable in practice if the illuminated region is small such that it can be approximated by a plane. In the next section we use the results presented here to analyze the ground clutter Doppler spread in airborne bistatic radar.

3.2 Doppler spread in ground clutter

The previous section gives the formula of the constant range contour on the ground, assuming flat earth. The illuminated portion of this contour defines the cross-range dimension of the range cell. In the following we derive the Doppler relationships along the aforementioned contour. It will be seen that the Doppler of the ground return is both range and angle dependent. The ground clutter Doppler spread is then analyzed.

Assume that the velocity of the transmitter is V_T, in the direction $(\cos\varphi_{V_T}\cos\theta_{V_T}, \sin\varphi_{V_T}\cos\theta_{V_T}, -\sin\theta_{V_T})$, and the velocity of the receiver is V_R, in the direction $(\cos\varphi_{V_R}\cos\theta_{V_R}, \sin\varphi_{V_R}\cos\theta_{V_R}, -\sin\theta_{V_R})$. The resulting Doppler at a point on the ground, $(x, y, -h_T)$, can be written as

$$\begin{aligned}
f_D &= \frac{V_T}{\lambda R_T}(x\cos\varphi_{V_T}\cos\theta_{V_T} + y\sin\varphi_{V_T}\cos\theta_{V_T} + h_T\sin\theta_{V_T}) \\
&\quad + \frac{V_R}{\lambda R_R}[(x - L_g)\cos\varphi_{V_R}\cos\theta_{V_R} + y\sin\varphi_{V_R}\cos\theta_{V_R} + h_R\sin\theta_{V_R}), \quad (3.10)
\end{aligned}$$

where λ is the wavelength. Figure 3.1 to Figure 3.3 show the constant Doppler contours using the same scenario as given in [16] but with the restriction of near zero altitude removed. The values used are $h_T = 0.1L, h_R = 0.2L$, $V_T = 100\text{m/s}$, $V_R = 250\text{m/s}$, $\theta_{V_T} = \theta_{V_R} = 0$, and $\lambda = 0.03\text{m}$. The unit of range in the figures is normalized with the baseline length. Fig. 3.1 depicts the case when $\varphi_{V_T} = \varphi_{V_R} = \pi/2$, while Figure 3.2 depicts the case $\varphi_{V_T} =$
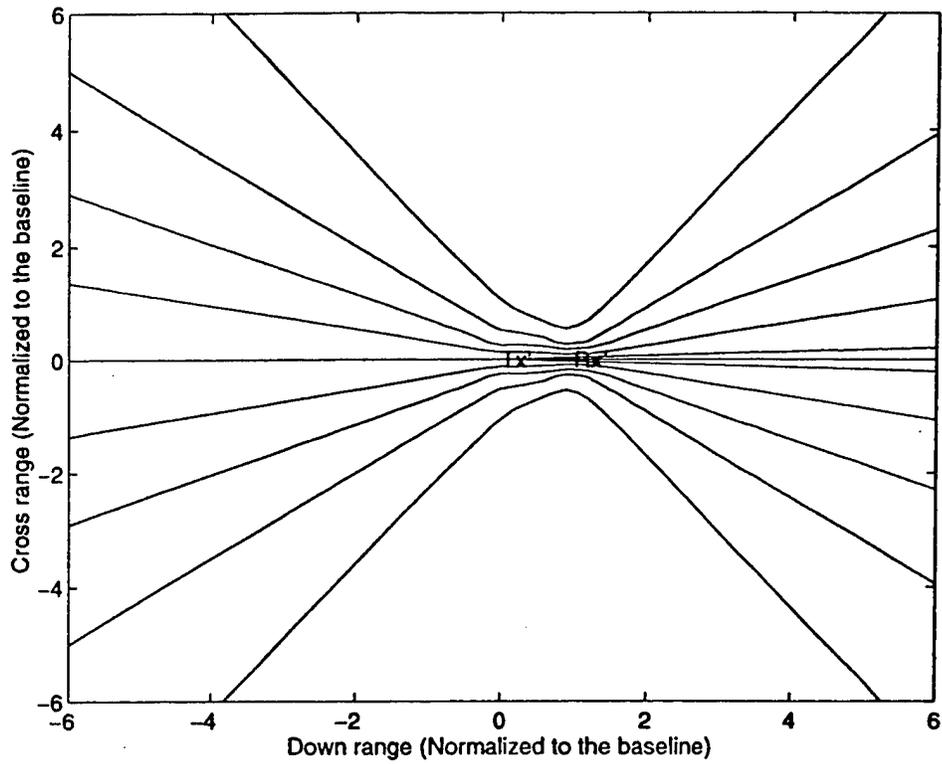
Figure 3.1: Bistatic constant Doppler contours on the bistatic plane
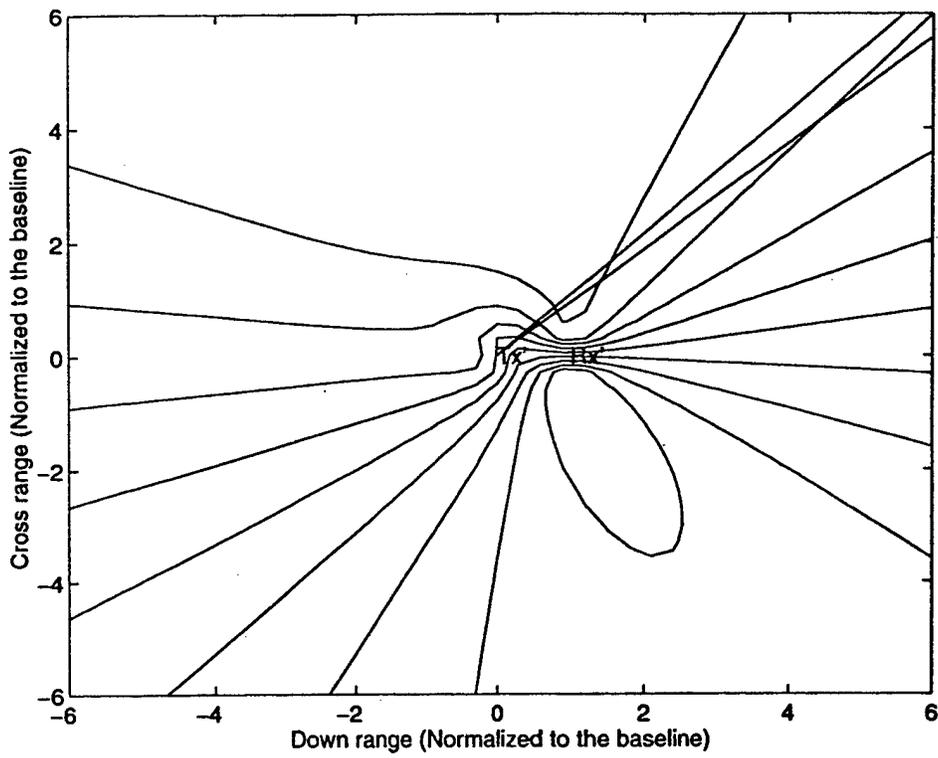
Figure 3.2: Constant Doppler contours on the ground for a bistatic radar with airborne transmitter

$\pi/2$. $\varphi V_R = 5\pi/4$. It can be seen from these figures that the Doppler shift varies along the ground projection of either the transmitter or the receiver line-of-sight. Consequently, collecting secondary data along either direction requires different Doppler compensations for each secondary range cell to reconcile with the clutter Doppler shift at the test cell. Nevertheless, the ground clutter Doppler spread may still depend on the range and angle. In the following we examine the Doppler spread at given transmitter and receiver azimuth angles.

The intersection of the transmitter line-of-sight and the constant range contour on the ground was given by (3.6) and (3.7). Substitution of these expressions into (3.10) gives the Doppler shift at that point. In other words, Doppler shift at the points on (3.2) is expressed as a function of the ranges and φ_T. Thus, writing the Doppler shift as $f_D(R, h_T, h_R, \varphi_T)$, it is easily seen that the maximum change in Doppler shift over the constant range contour, within the transmitting beam, can be obtained by

$$\Delta f_{D_T} = \max_{\varphi_T \in D_{B_T}} f_D(R, h_T, h_R, \varphi_T) - \min_{\varphi_T \in D_{B_T}} f_D(R, h_T, h_R, \varphi_T), \tag{3.11}$$

where D_{B_T} is the interval of φ_T of the transmitting beam. In fact, Δf_{D_T} is the ground clutter Doppler spread when the cross-range dimension of the transmitting beam is the determining factor of the cell length. Likewise, substitution of (3.8) and (3.9) into (3.10) may be used to calculate the clutter Doppler spread when the cell length is determined by the receiving beam:

$$\Delta f_{D_R} = \max_{\varphi_R \in D_{B_R}} f_D(R, h_T, h_R, \varphi_R) - \min_{\varphi_R \in D_{B_R}} f_D(R, h_T, h_R, \varphi_R), \tag{3.12}$$

where D_{B_R} is the interval of φ_R of the receiving beam.

In the following we give an example to illustrate how the Doppler spread varies along a given direction of the transmitting beam; similar results can be expected along a given receiving beam direction. The beam width is assumed to be 4 deg and the geometry in Figs. 3.1 and 3.2 are used. Figures 3.3 and 3.4 show the Doppler spread for $\varphi_T = 0$ deg and $\varphi_T = 45$ deg, respectively.

In this section we derived the Doppler shift along a constant range contour on the ground for an airborne bistatic radar. It was shown that the Doppler shift is both range and
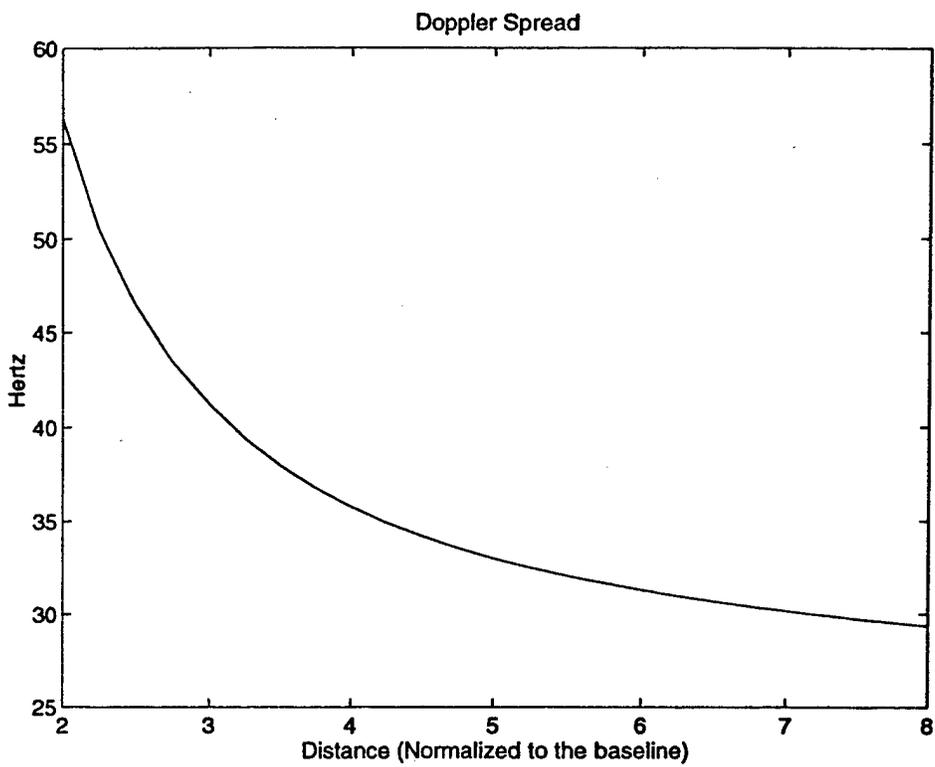
Figure 3.3: Clutter Doppler spread along the direction of $\varphi_T = 0 \deg$
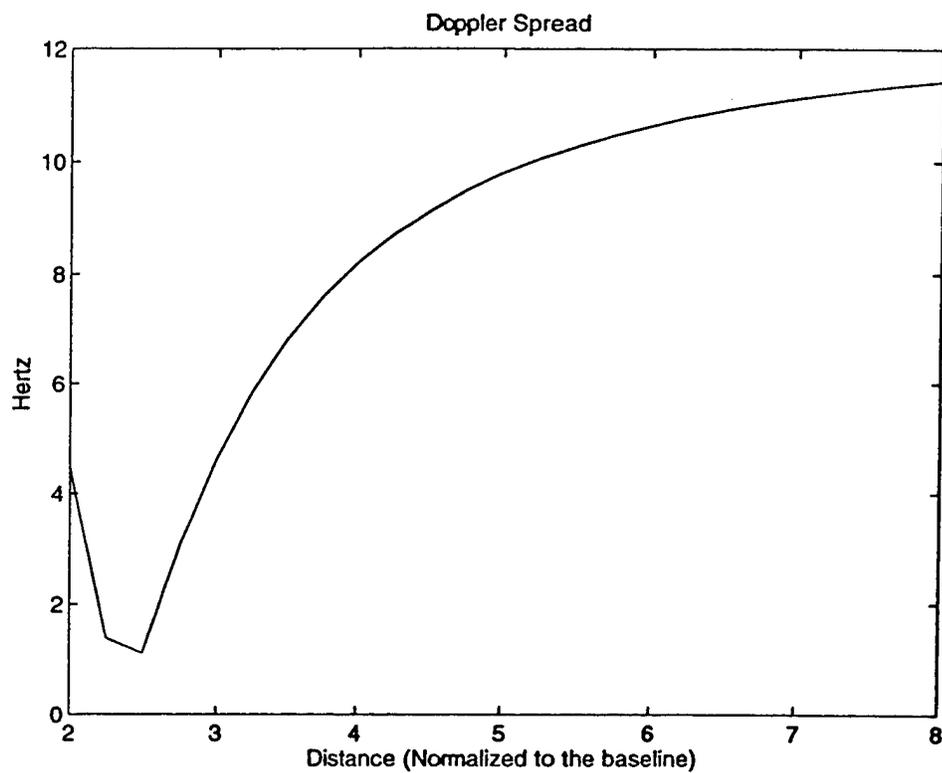
Figure 3.4: Clutter Doppler spread along the direction of $\varphi_T = 45\,\mathrm{deg}$

angle dependent. The clutter Doppler spread along a given transmitting or receiving beam direction was then analyzed. The results were illustrated with an example. In the next chapter we examine how the variation in the clutter spread affects the estimation of the clutter covariance matrix.

Chapter 4

A Preliminary Study of Space-Time Processing for Multistatic Radar System

In this chapter we present some results from a preliminary study of the space-time processing for multistatic system. This analysis will provide us with a basis for further development. Attention is restricted to the single transmitter case. The extension to a more generalized system is straightforward and involves the same concept.

Optimum processing and the steering signal

Suppose the multistatic system consists of one transmitter and M receivers. The returned signal vector is now given as $\tilde{s} = [\tilde{s}_1^T \tilde{s}_2^T \cdots \tilde{s}_M^T]^T$, where $\tilde{s}_m, m = 1, 2, \cdots, M$, is the signal sample vector obtained at the mth receiver. The vectors of the noise and the weights of the optimum filter can be formed in a similar manner.

On the one hand, using the Schwarz inequality, the same conclusion can be drawn that the optimum filer weights are of the form given by (1.2); on the other hand, a direct realization may be prohibitive due to the heavy computational requirement. It is of interest to find out the possibility of further simplifying (1.2).

Assume the interferences from different receivers have zero mean and are uncorrelated

such that

$$R_n = \mathrm{E}\dot{n}\tilde{n}^H = \begin{bmatrix} R_{n_1} & 0 & \cdots & 0 \\ 0 & R_{n_2} & & \\ \vdots & & \ddots & \\ 0 & & & R_{n_M} \end{bmatrix} \tag{4.1}$$

where $R_k, k = 1.2, \cdots, M$ are the noise covariance matrix of the kth receiver and 0 is a zero matrix. It follows that

$$R_n^{-1} = \begin{bmatrix} R_{n_1}^{-1} & 0 & \cdots & 0 \\ 0 & R_{n_2}^{-1} & & \\ \vdots & & \ddots & \\ 0 & & & R_{n_M}^{-1} \end{bmatrix} \tag{4.2}$$

Substituting the above into (1.2), we see that the optimum weights of each receiver can be generated independently.

The use of (4.2) relies on whether it is appropriate to assume that the noise at one receiver is independent from that from the others. In fact, such assumption is applicable when the thermal noise is dominant, but it may not be suitable when clutter is the prevailing factor of the interference. This is one of the problem to be solved in developing space-time processing for multistatic radar.

There is another problem generally overlooked, namely, the employment of equally spaced array sensors. This configuration may not cause difference in the monostatic case, where geometry does not change the clutter characteristics. However, the analysis in Chapter 2 indicates that the bistatic geometry affects the observed clutter characteristics. Consequently, array sensors that are not equally spaced may be more suitable for the application of space-time processing in the bistatic/multistatic case. This problem is to be analyzed.

Chapter 5

Discussion

In this report, we presented an analysis of the clutter characteristics as observed from a radar platform of either the monostatic or the bistatic configuration, airborne or stationary. This study shows the effects of system parameters, particularly the system geometry, on the observed clutter characteristics. However, due to the lack of a suitable model, variation of the clutter strength in the out-of-plane geometry in the bistatic radar was not included. This problem will be considered further in the next phase of this research effort.

A preliminary study of adaptive space-time processing for multistatic active radar can be found in this report as well. This analysis shows where the problems lie and provides us with a basis for further development. It is seen that there are two major factors that need to be investigated further in the development of space-time processing for the multistatic system: (1) the correlation of the observed interference among the receivers; and (2) the effects of system geometry on the observed reverberation characteristics.

As the analysis shown, the problem of multistatic space-time processing reduces to the monostatic one when the interferences are uncorrelated. However, this may not be the case, e.g., when multipath occurs. Then, it is of interest to know if the a priori knowledge of the system geometry can be used to reduce the computational burden. It was also seen from the study of clutter characteristics that the observed clutter characteristics does depend on the system geometry. stationary. Then, the question is how it affects the system performance and if it can be rectified. Problem also arises when the actual signal angle of arrival does not coincide with the estimated one, or when the actual geometry of the array differs from

the one assumed. When such errors occur, the actual signal may be tuned out, instead of the intended interference.

The aforementioned issues are essential to the bistatic/multistatic space-time processing. They need to be addressed before an effective system can be implemented. The solution to them is the goal of the next phase of this research effort.

Bibliography

[1] L. E. Brennan and I. S. Reed, "Theory of Adaptive Radar". *IEEE Trans. Aero. Elec. Sys.*, vol. AES-9, pp. 237-252, 1973.

[2] P. K. Varshney *et al.*, *Analysis of Ambiguity Function for Bistatic Radar*, Rome Laboratory, Rome, N.Y., Technical Report No. RL-TR-95-23, 1995.

[3] H. L. Van Trees, "Optimum Signal Design and Processing for Reverberation-Limited Environments", *IEEE Trans. Military Electronics*, vol. MIL-9, pp. 212-229, July-Oct., 1965.

[4] K. J. Sangston and K. R. Gerlach, "Coherent Detection of Radar Targets in a Non-Gaussian Background", *IEEE Trans. Aero. Elec. Sys.*, vol. AES-30, pp. 330-340, 1994.

[5] A. W. Rihaczek, *Principles of High Resolution Radar*, New York: McGraw-Hill, 1969, pp. 331-349.

[6] D. Middleton, "A Statistical Theory of Reverberation and Similar First-Order Scattered Fields, Part I: Waveforms and General Process", *IEEE Trans. Info. Theory*, vol. IT-13, pp. 372-392, July, 1967.

[7] ———, "A Statistical Theory of Reverberation and Similar First-Order Scattered Fields, Part II: Moments, Spectra, and Special Distributions", *IEEE Trans. Info. Theory*, vol. IT-13, pp. 372-392, July, 1967.

[8] ———, "A Statistical Theory of Reverberation and Similar First-Order Scattered Fields, Part III: Waveforms and Fields", *IEEE Trans. Info. Theory*, vol. IT-18, pp. 35-67, Jan., 1972.

[9] ——. "A Statistical Theory of Reverberation and Similar First-Order Scattered Fields, Part IV: Statistical Models", *IEEE Trans. Info. Theory*, vol. IT-13, pp. 68-90, Jan., 1972.

[10] ——. "Doppler Effects for Randomly Moving Scatterers and platforms" *Journal of the Acoustical Society of America*, vol. 61, pp. 1231-1250, may, 1977.

[11] H. L. Van Trees, *Detection, Estimation, and Modulation Theory, Part III*, Norwood, Mass: Artech House, 1971.

[12] R. Klemm. "MTI", *Proc. IEE, Part F*, vol. IT-13, pp. 1231, July, 1983.

[13] Barbarossa and Farina, "Space-Time-Frequency Processing", *IEEE Trans. Aero. Elec. Sys.*. vol. AES-13, pp. 372-392, July, 1994.

[14] Barton. "Space-Time-Frequency Processing", *Proc. IEEE*, vol. AES-13, pp. 372-392, July. 1985.

[15] D. C. Schleher, *MTI and Pulsed Doppler Radar*, Artech House, Norwood, MA, 1991.

[18] H. M. Finn and R. S. Johnson, "Adaptive Detection Mode with Threshold Control as a Function of Spatially Sampled Clutter-Level Estimates," *RCA Rev.*, vol. 29. pp. 414-464, Sept. 1968.

[19] E. J. Kelly. "An Adaptive Detection Algorithm," *IEEE Trans. Aero. Elec. Sys.*. vol. AES-22, pp. 115-127, 1986.

Appendix A

Some Results on Bistatic Geometry

Here we give a detailed derivation of the geometry relationships for bistatic radar. Some special cases are considered for illustration.

A.1 Relationships among the distance parameters

From (2.43). (2.54) and (2.55), it can be shown that

$$R_T = \left[R(R^2 + B) + A\sqrt{(R^2 + B)^2 - 4h_T^2(R^2 - A^2)}\right] \Big/ \left[2(R^2 - A^2)\right] \qquad (A.1)$$

for $R \geq h_T + \sqrt{L^2 \cos^2 \theta_{RT} + h_R^2}$, and

$$R_T = \left[R(R^2 + B) \pm A\sqrt{(R^2 + B)^2 - 4h_T^2(R^2 - A^2)}\right] \Big/ \left[2(R^2 - A^2)\right] \qquad (A.2)$$

for $R < h_T + \sqrt{L^2 \cos^2 \theta_{RT} + h_R^2}$. Using the definition that $R = R_T + R_R$. it follows that

$$R_R = \left[R(R^2 - 2A^2 - B) - A\sqrt{(R^2 + B)^2 - 4h_T^2(R^2 - A^2)}\right] \Big/ \left[2(R^2 - A^2)\right] \qquad (A.3)$$

for $R \geq h_T + \sqrt{L^2 \cos^2 \theta_{RT} + h_R^2}$, and

$$R_R = \left[R(R^2 - 2A^2 - B) \mp A\sqrt{(R^2 + B)^2 - 4h_T^2(R^2 - A^2)}\right] \Big/ \left[2(R^2 - A^2)\right] \qquad (A.4)$$

for $R < h_T + \sqrt{L^2 \cos^2 \theta_{RT} + h_R^2}$.

Differentiating (2.55), we have

$$\frac{dR_{T_\theta}}{dR} = \Big\{-2AR(A^2 + B)\sqrt{(R^2 + B)^2 - 4h_T^2(R^2 - A^2)}$$
$$\pm \left[R^6 - 3A^2R^4 - (4A^2B + B^2 - 4A^2h_T^2)R^2 - (A^2B^2 + 4A^4h_T^2)\right]\Big\}$$
$$\cdot \left[2(R^2 - A^2)^2\sqrt{(R^2 + B)^2 - 4h_T^2(R^2 - A^2)}\right]^{-1}. \qquad (A.5)$$

The subtraction in (A.5) only occurs when $R < h_T + \sqrt{L^2 \cos^2 \theta_{RT} + h_R^2}$. Using the results for R_T and R_R, we have

$$\frac{dR_{T_g}}{dR} = \pm 2 R_T R_R \left[(R^2 + B)^2 - 4 h_T^2 (R^2 - A^2) \right]^{-1/2} \tag{A.6}$$

the negative sign only occurs when $R < h_T + \sqrt{L^2 \cos^2 \theta_{RT} + h_R^2}$.

Special cases

Clearly, the parameters for the monostatic case can be obtained by letting $L = 0$, and they are not derived here. When $h_T = 0$,

$$R_T = (R^2 - L^2) / \left[2(R - L \cos \theta_{RT} \sin \varphi_T) \right], \tag{A.7}$$

$$R_R = [R^2 - 2L^2 \cos^2 \theta_{RT} \sin^2 \varphi_T + h_R^2 + L^2 \cos^2 \theta_{RT}] / 2(R - L \cos \theta_{RT} \sin \varphi_T), \tag{A.8}$$

$$R_{T_g} = R_T, \tag{A.9}$$

and

$$\frac{dR_T}{dR} = \frac{dR_{T_g}}{dR} = 2 R_T R_R / (R^2 - L^2) \tag{A.10}$$

A.2 Width of the range ring and the distance to the receiver

From the definition that $R = R_T + R_R$, we have

$$\frac{dR_R}{dR} = 1 - \frac{dR_T}{dR}. \tag{A.11}$$

It follows that

$$\frac{dR_R}{R_R} = \left(1 - \frac{dR_T}{dR} \right) \frac{dR}{R_R}. \tag{A.12}$$

Using (2.54), (2.67) and (A.3) in (A.12), we have

$$\frac{dR_R}{R_R} = \left\{ \frac{2(1 - A^2/R^2)}{1 - 2A^2/R^2 - B/R^2 - (A/R)\sqrt{(1 + B/R^2)^2 - 4h_T^2/R^2(1 - A^2/R^2)}} \right.$$
$$\left. - \frac{(A/R)(1 + B/R^2) + \sqrt{(1 + B/R^2)^2 - 4h_T^2/R^2(1 - A^2/R^2)}}{(1 - A^2/R^2)\sqrt{(1 + B/R^2)^2 - 4h_T^2/R^2(1 - A^2/R^2)}} \right\} \frac{dR}{R}. \tag{A.13}$$

Invoking the assumptions that the square of the ratios h_T/R, h_R/R and L/R are much smaller than unity, the above relationship reduces to

$$\frac{dR_R}{R_R} = \frac{1}{1 - A/R}\frac{dR}{R}.$$

(A.14)

Also, following the assumptions, the second and higher powers of $|A/R|$ are much smaller than unity; thus,

$$\frac{dR_R}{R_R} = \left(1 + \frac{A}{R}\right)\frac{dR}{R}.$$

(A.15)

Since $|A/R|$ is smaller than unity, we conclude that $\triangle R_R/R_R \ll 1$ when $\triangle R/R \ll 1$ within one range ring.

MISSION
OF
AFRL/INFORMATION DIRECTORATE (IF)

The advancement and application of information systems science and technology for aerospace command and control and its transition to air, space, and ground systems to meet customer needs in the areas of Global Awareness, Dynamic Planning and Execution, and Global Information Exchange is the focus of this AFRL organization. The directorate's areas of investigation include a broad spectrum of information and fusion, communication, collaborative environment and modeling and simulation, defensive information warfare, and intelligent information systems technologies.